FORMATION OF Au NANOPARTICLES THROUGH REDUCTION OF $Na_3Au(SO_3)_2$ BY ELECTROCHEMICALLY EVOLVED HYDROGEN

by

YI JIUN LI

Presented to the Faculty of the Graduate School of

The University of Texas at Arlington in Partial Fulfillment

of the Requirements

for the Degree of

MASTER OF SCIENCE IN MATERIALS SCIENCE AND ENGINEERING

THE UNIVERSITY OF TEXAS AT ARLINGTON

May 2010

ACKNOWLEDGEMENTS

I sincerely thank Dr. Seong Jin Koh and Dr. Fuqiang Liu for their support, reviewing my thesis and being my committee member, and also give my appreciation to all the professors in the Department of Material Science and Engineering for offering their knowledge and guidance. I express my gratitude to administrative secretaries, Jennifer Standlee and Libia Cuauhtli, for their contribution in my academic paper works.

I'm truly grateful for my advisor, Dr. Yaowu Hao, who gave me valuable advice and suggestions with his immense experience and knowledge, and led me from initial to final level enabled me to develop an understanding of the subject. The thesis would not have been possible without his guidance. It is my pleasure to thank Nanofab staffs, Dr. Fatima Z. Amir, Mr. Eduardo Maldonado and Mr. Dennis Bueno who trained me on various facilities and assistance in equipment.

My sincere thanks I would also like to bestow upon my group members: Chien-Wen Huang who taught me electrochemical knowledge and basic laboratory skills, Punnapob Punnakitikashem who assisted me with anodic oxidation, Shih-Hsin Chang, Chivarat Muangphat, Orathai Thumthan and Megha Panuganti for sharing their erudition. I have enjoyed the atmosphere we have created together in the lab. It is an honor for me to express my appreciation to my friends, Chenchi Kuo, Jinwen He and Craig Allen Epp who encouraged and supported me.

Last but not the latest, I would like to devote the heartiest appreciation to my parents and sister for supporting me spiritually throughout my life.

April 14, 2010

ABSTRACT

FORMATION OF Au NANOPARTICLES THROUGH REDUCTION OF $Na_3Au(SO_3)_2$ BY ELECTROCHEMICALLY EVOLVED HYDROGEN

Yi Jiun Li, M.S.

The University of Texas at Arlington, 2010

Supervising Professor: Yaowu Hao

Hydrogen evolution during electrochemical deposition has long been regarded as undesired and deliberately suppressed since small hydrogen bubbles could cause a rough surface of deposits. Here, we demonstrate a new role for electrochemically evolved hydrogen, serving as both templates and reducing agents for synthesizing Au nanoparticles via electroless depositions from $Na_3Au(SO_3)_2$ electrolytes.

A series of experiments have been designed to investigate this new role. A working electrode of patterned Ag strips on the non-conductive substrates has been used. It has been observed that when a potential more negative than hydrogen evolution potential was applied to metal areas, a large amount of Au nanoparticles formed on the non-conductive regions. This strongly suggests that hydrogen evolution and electroless deposition play critical roles for the formation of Au nanoparticles. Au nanoparticles have also been generated on TEM grid, which provided a convenient way for analyzing the structure of Au nanoparticles. The hollow feature of Au nanoparticles was revealed by high-resolution transmission electron microscopy (HRTEM) suggesting electrochemically evolved hydrogen bubbles act as templates for the formation of Au nanoparticles.

It has been found that the size and size distribution of Au nanoparticles were affected by applied potential and addition of Ni^{2+} ions in the electrolyte. The higher applied potential usually results in larger hydrogen bubbles thus a bigger size of Au nanoparticles. Ni^{2+} ions can enhance hydrogen evolution efficiency which gives the better size distribution of Au nanoparticles. Moreover, the effects of hydrophobicities of substrates have been studied. It shows that Au nanoparticles can form on both hydrophobic and hydrophilic surfaces, and the hydrophobicity does not have effects on the morphology of Au nanoparticles. This result is not fully understood, and more studies are needed to investigate the formation mechanisms of nanobubbles on different substrates. Au metal formation around electrochemically evolved hydrogen bubbles has been directly observed. However, no reaction takes place around hydrogen gas bubbles. This may be due to that hydrogen gas bubbles are less reactive than electrochemically hydrogen bubbles.

TABLE OF CONTENTS

LIST OF ILLUSTRATIONS

LIST OF TABLES

CHAPTER 1

INTRODUCTION

Hydrogen evolution could cause extremely rough deposits during electrochemical deposition due to tiny small hydrogen bubbles generate on electrode surfaces [1]. Therefore, hydrogen evolution has been regarded as undesired and deliberately suppressed. Recently, we have successfully demonstrated that electrochemically evolved hydrogen nanobubbles can serve as both templates and reducing agents for synthesizing Au nanoparticles via electroless deposition from $Na_3Au(SO_3)_2$ electrolytes.

In order to study this process, non-conductive substrates were patterned with periodical Ag strips. The metal strips served as the working electrode, and the non-conductive areas were used to observe the electroless reaction. On the strip-patterned substrates, we observed a large amount of Au nanoparticles formed on the non-conductive areas when a potential applied to the metal strips was more negative than hydrogen evolution potential. Since electrochemical deposits can only occur on electrode surface, electroless deposition should be the only possible reason for the formation of Au nanoparticles on the non-conductive areas.

The mechanism of Au nanoparticles formation has been systematically studied. The formation of hollow Au nanoparticles could be described as a three-stage process. In the first stage, at a certain potential, hydrogen evolution starts, and hydrogen nanobubbles form on the substrate surfaces. The second stage is the reduction of Au^+ into metallic gold by hydrogen nanobubbles. The reduction takes place at the hydrogen bubble boundary. In the last stage, autocatalytic disproportionation reaction occurs in the gold(I) sulfite electrolyte.

The effects of stabilizer, additive, potential and hydrophobicity of substrates on the formation of Au nanoparticles have been investigated. The stability of electrolytes plays important roles in the synthesis process. It has been investigated in both gold(I) cyanide and

gold(I) sulfite electrolyte solutions. As expected, only Au^{+} in sulfite complex was able to be reduced by electrochemically evolved hydrogen bubbles. It shows that stabilizer (EDA), a key additive, was not only able to stabilize the electrolytes, but also able to clean surface oxides from active metal of electrode, and thus lead to the increase of hydrogen evolution efficiency. It has been found that the size distribution of Au nanoparticles was improved by the addition of Ni^{2+} ions in the electrolyte. The cyclic voltammetry measurement revealed that the newly deposited Ni metal on electrode surface was able to enhance hydrogen evolution, which may contribute to the better size distribution of Au nanoparticles. Hydrogen evolution is directly related to applied potential, therefore, the size of nanoparticles are affected by applied potentials. Various substrates with different hydrophobicities have been used to study the morphologies of Au nanoparticles. It suggests that the hydrophobicities of solids do not affect the contact angle of nanobubbles, which is not fully understood and requires more studies.

Au nanoparticles have also been produced on a TEM grid which provided a convenient way for analyzing the structure of Au nanoparticles. The hollow feature of Au nanoparticle was revealed by high-resolution transmission electron microscopy (HRTEM), suggesting electrochemically evolved hydrogen bubbles act as templates for the formation of Au nanoparticles. We have directly observed Au metal formation around electrochemically evolved hydrogen bubbles. However, reduction does not take place around hydrogen gas bubbles. We speculated that hydrogen gas bubbles are less reactive than electrochemically evolved hydrogen bubbles.

CHAPTER 2

BACKGROUND

2.1 Synthesis and Optical Properties of Au Nanoparticles

Gold nanoparticles have captured the attention from researchers in various disciplines due to the fact that their optical properties can be tuned by adjusting the shape and size [2-7]. The unique optical property of Au nanoparticles arises from surface plasmon resonance (SPR) effect. SPR occurs from the interaction between the conduction electrons in a metal and electromagnetic field. When the size of nanoparticle is much smaller than the wavelength of the incident light, an electromagnetic field at a certain frequency induces a resonant; coherent oscillation of the metal free electrons across the nanoparticle as shown in Figure 2.1. This oscillation is known as surface plasmon resonance.

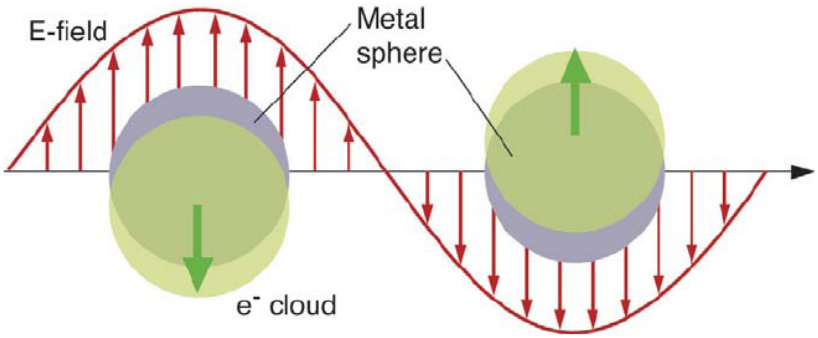

Figure 2.1 The electromagnetic field of the light induces a coherent dipolar oscillation of the metal conduction electrons across the nanoparticle.

Au nanoparticles are mainly classified into spherical nanoparticles [8], nanorods [9, 10], nanocages [11] and nanoshells [12, 13] by their morphology. The synthesis was mainly approached by chemical methods, including galvanic replacement, diffusion, oxidation, and ion

exchange [14]. The characteristics and synthesis of different shapes of Au nanoparticles and their optical properties will be reviewed in this section.

2.1.1 Spherical Au Nanoparticles

Among several conventional chemical methods for reduction of gold(III), the most popular method is citrate reduction of $HAuCl_4$ in water (Equation 2.1) which was proposed by Trukevitch in 1951 [15]. It is well known from this method that chemical reduction of gold salts produces spherical Au nanoparticles (Equation 2.1).

$$6AuCl^-_4 + C_6H_8O_7 + 5H_2O \rightarrow 6CO_2 + 24Cl^- + 6Au^0 + 18H^+ \quad (2.1)$$

The size of Au nanoparticles (between 16 - 147nm) can be controlled by the ratio between the reducing and stabilizing agents [16]. The Brust-Schiffrin [17] reported two phase liquid-liquid system for synthesizing thiol-derivatized Au nanoparticles. It has had a considerable impact on the overall field because it allowed the facile synthesis of thermally stable and air-stable Au nanoparticles with controlled size. The technique is based on the fact that thiol ligands strongly bind gold due to the strong affinity between Au and S. $AuCl^-_4$ is transferred to toluene using tetraoctylammonium reduced by $NaBH_4$ in the presence of dodecanethiol (Figure 2.2). Using such strategies, it is possible to generate dispersed spherical nanoparticles with high quality.

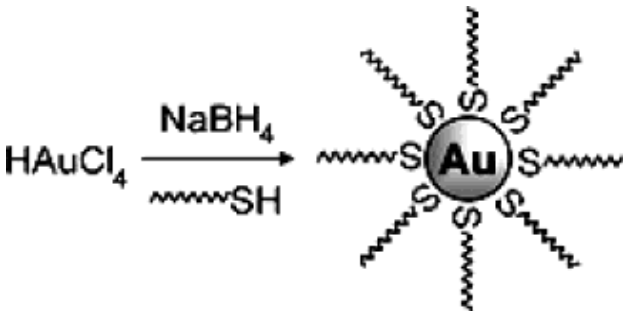

Figure 2.2 Formation of Au nanoparticles coated with organic shells by reduction of Au(III) compounds in the presence of thiols [18].

Spherical Au nanoparticles can experience surface plasmon resonance in the visible portion of the spectrum. This means that a certain portion of visible wavelengths will be absorbed, while another portion will reflected. The portion reflected will lend the material a

certain color. Small nanoparticles (40 - 100nm) absorb light in the blue-green portion of the spectrum while red light is reflected. As particle size increases (100 – 140nm), the wavelength of surface plasmon resonance related absorption shifts to longer wavelengths. This means that red light is now adsorbed, and bluer light is reflected, yielding particles with a blue color. As particle size continues to increase toward the bulk limit, surface plasmon resonance wavelengths move into the near infrared portion of the spectrum and most visible wavelengths are reflected.

2.1.2 Au Nanorods

Au nanorods have been prepared using template-directed, electrochemical reduction [9] and seed-mediated methods. Among them, template-directed method is commonly used [9, 19-22].

The template method is based on the electrochemical deposition of Au within the pores of alumina templates [21], polycarbonate templates [19], or carbon nanotube templates [22]. Au nanorods with different diameters can be prepared by controlling the pore diameter of the template and the length of nanorods can be controlled through the amount of Au deposited within pores (Figure 2.3) [21].

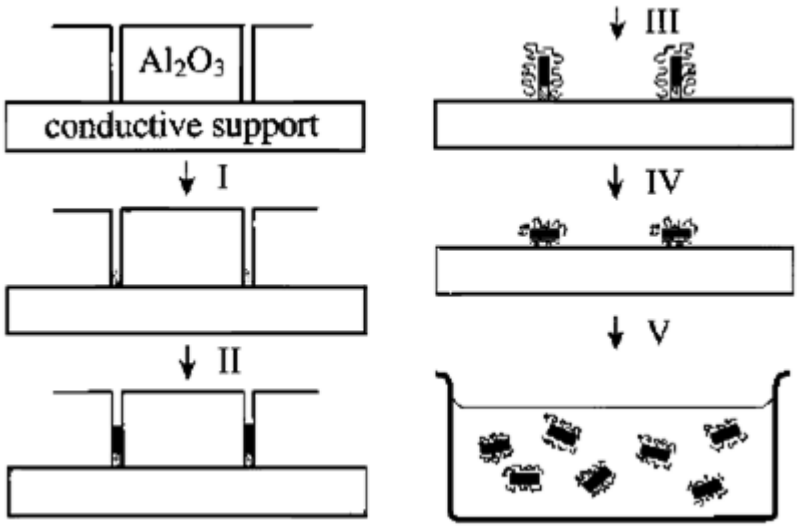

(a)

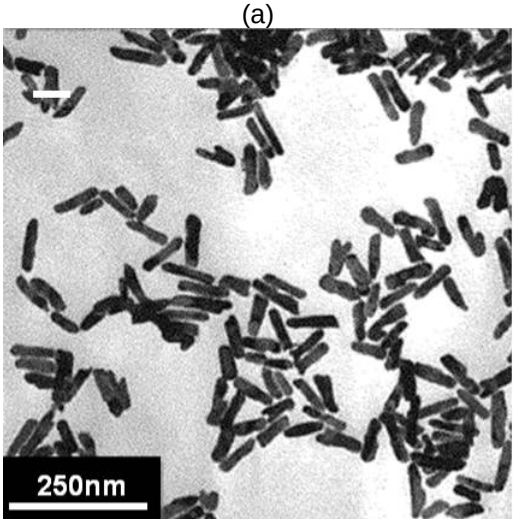

(b)

Figure 2.3 (a) Schematic representation of the successive stages to obtain aqueous dispersions of Au rods: (I) starting from the alumina membrane, (II) involves the electrodeposition of Au, (III) and (IV) the membrane and the supporter are selectively dissolved to release the rods, (V) the rods are dispersed in water by ultrasonication; (b) TEM micrographs of Au nanorods obtained by the template method [21].

In the electrochemical reduction method, a simple two-electrode-type electrochemical cell is used (Figure 2.4a). An Au metal plate is used as a sacrificial anode, and the cathode is a platinum plate. Both electrodes are immersed in an electrolyte containing cationic surfactant, hexadecyltrimethylammonium bromide (C_{16}TAB), and a small amount of hydrophobic cationic

surfactant, tetradodecylammonium bromide ($TC_{12}AB$). $C_{16}TAB$ serves not only as the supporting electrolyte, but also as the stabilizer for preventing aggregation of nanoparticles. During the synthesis, the bulk Au is converted to Au complex ions $AuBr^-_4$ by external current. The reduction reaction participates at the interfacial region between the cathode and the electrolyte. The Au complex ions may combine with the cationic surfactants to facilitate the formation of rod-like Au nanoparticles (Figure 2.4b) [9].

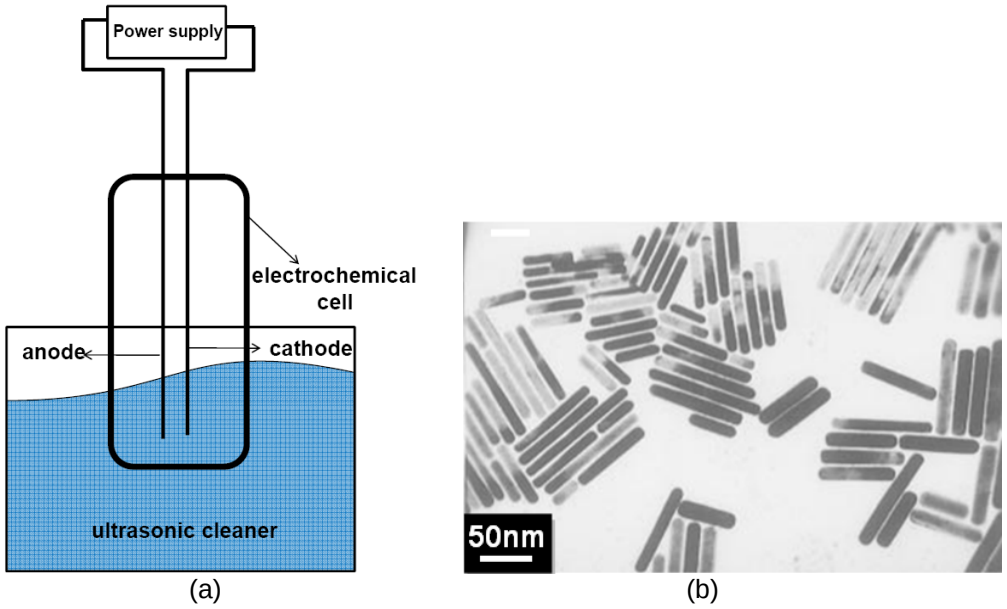

Figure 2.4 (a) Schematic diagram of the setup for preparation of Au nanorods via the electrochemical method; (b) TEM micrographs of Au nanorods with aspect ratio 6.1 [9].

Seeded growth method uses the approach of step-by-step particle enlargement, which allows the ratio of seeds to metal salts to be maintained throughout successive growth steps [23]. Murphy [24] used this approach to synthesize high aspect ratio cylindrical nanorods. The primary nuclei are 3.5nm Au seeds prepared by reducing $HAuCl_4$ with sodium borohydride ($NaBH_4$) in the presence of citrate which works as a capping agent [25]. The growth steps are carried out in aqueous surfactant media. Secondary growth stage is inhibited by carefully controlling the growth conditions. $HAuCl_4$ and $C_{16}TAB$ are mixed with ascorbic acid, a weak reducing agent that cannot reduce the Au salt in the presence of the micelles without the seed,

and then added to a seed solution to generate Au nanorods. Although Au nanospheres are also formed in this synthesis, they can be readily removed *via* centrifugation (Figure 2.5) [26]. It was found that the addition of $AgNO_3$ could influence the yield and aspect ratio control of the Au nanorods.

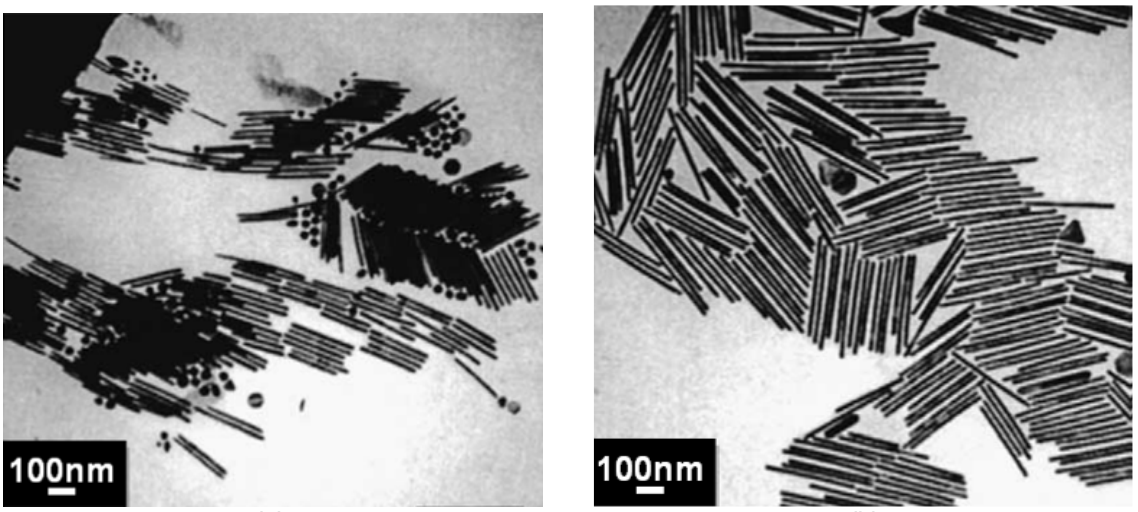

(a) (b)

Figure 2.5 TEM micrographs of: (a) before shape-separated Au nanorods; (b) after shape-separated Au nanorods prepared by the seed-mediated method [26].

The SPR peak of Au nanorods falls into two ranges due to the orientations of the rod with respect to the electric field of incident light. A SPR peak around 530nm corresponds to the transverse plasmon oscillation and stronger SPR peak at near-infrared region arising from the plasmon oscillation along the longitudinal axis of the nanorods [2, 5].

2.1.3 Au Nanocages

Xia and co-workers [11] used monodisperse poly(vinyl)pyrollidone (PVP) stabilized Ag nanocubes which serves as a template for galvanic replacement with $HAuCl_4$, resulting in hollow Au nanostructures with controlled void size and shell thickness. Ag nanocubes suspended in solution can be oxidized and replaced by $HAuCl_4$ according to the following replacement reaction.

$$3Ag_{(s)} + AuCl^-_{4(aq)} \rightarrow Au_{(s)} + 3Ag^+_{(aq)} + 4Cl^-_{(aq)} \quad (2.2)$$

The silver nanocubes are prepared using a polyol process[27], and then the silver nanocubes react with the $HAuCl_4$ to form small holes on a specific face. As reaction continues, Au atoms are deposited on the surface of the silver nanocube to generate a thin shell. The Ag atoms can also diffuse into the gold shell, leading to the formation of a closed box made of Au/Ag alloy (Figure 2.6) [11]. This eventually led to the formation of a hole at each corner of the nanoboxes as show in (Figure 2.7) [11].

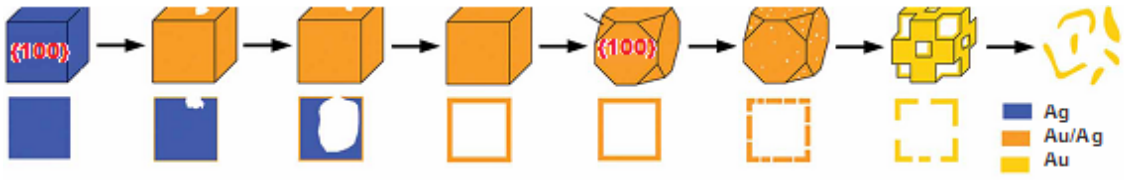

Figure 2.6 Schematic illustrations of synthesized hollow nanostructures from Ag nanocubes with increasing amounts of $HAuCl_4$ solution. (1) initiation of replacement reaction at a specific site with the highest surface energy, (2) continuation of the replacement reaction and the formation of a partially hollow nanostructure, (3) formation of nanocages with a uniform and homogeneous wall composed of Au/Ag alloy, (4) initiation of dealloying and corner reconstruction of the Au/Ag nanocages, (5,6) continuation of dealloying and formation of an Au nanocages with pores in the walls [11].

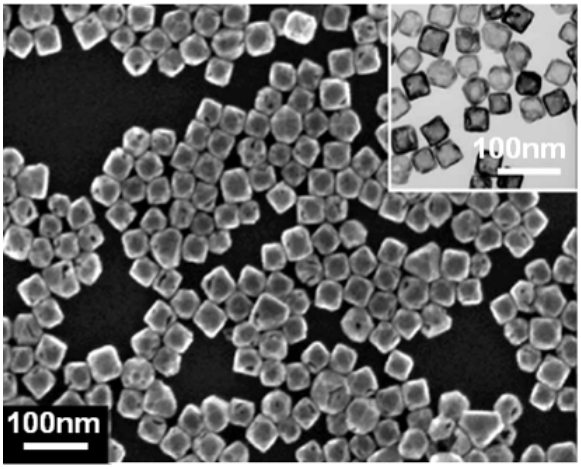

Figure 2.7 SEM micrograph of Au nanocages prepared through the galvanic replacement reaction; sub-image, TEM micrograph, shows the contrast of interior void [11].

The SPR peaks of Au nanocages could be shifted in a spectral region from 400 to 1200nm by controlling the molar ratio of Ag to $HAuCl_4$. Moreover, Au nanocages with SPR

peaks in the near-infrared region exhibited a broad two-photon photoluminescence band extending from 450 to 650nm when excited by a sapphire laser at 800nm [28-30].

2.1.4 Au Nanoshells

Halas and co-workers [11] have developed a method to make gold nanoshells on silica treated with triethoxysilane. In this process, uniform silica spheres are first synthesized using the Stöber method. The surfaces of silica beads are then modified with a monolayer of amino-terminated silane. The gold shell is grown on the silica cores via the seed-mediated electroless plating. First, small gold colloids (~2nm), are attached to the amine-terminated silica surfaces. Gold is electrolessly plated onto the colloidal nucleation sites from diluted solution of gold chloroauric ($HAuCl_4$) and potassium carbonate (K_2CO_3) using formaldehyde (CH_2O) as a reduction agent. The thickness of shell is controlled by the relative amounts of silica core and the Au salt solutions. Generally, a continuous Au shell has a thickness between 5 – 30nm (Figure 2.8) [11].

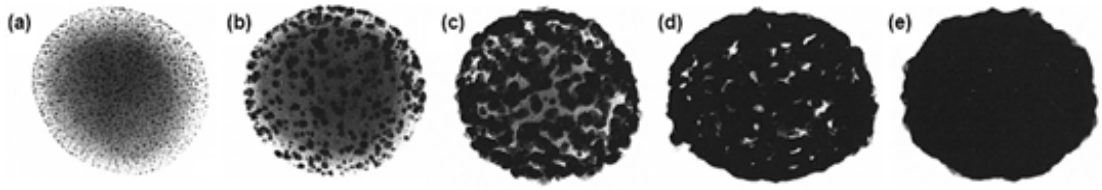

Figure 2.8 TEM micrographs of nanoshells growth on 120nm diameter silica dielectric nanoparticles: (a) initial gold colloid-decorated silica nanoparticles, (b) - (d) gradual growth and coalescence of gold colloid on silica nanoparticle surface, (e) completed growth of metallic nanoshells [11].

There are a few reports showing fabrications of gold shells with other materials as the core. Polystyrene spheres have been particularly useful for the formation of photonic crystals. The higher refractive index of polystyrene, compared to that of silica, also results in a somewhat narrower plasmon resonance absorption peak for gold shells on polystyrene compared to that for gold shells on silica. Use of polystyrene spheres as the core in these structures is advantageous because they are readily available commercially in a wide range of sizes, and

with dyes or other molecules doped into them [31]. Uniform polystyrene spheres are first synthesized. The surfaces of polystyrene are then modified. Second, the small gold colloids are grown on the polystyrene cores via the seed-mediated electroless plating from gold chloroauric acid ($HAuCl_4$) with reduction agent [32] (Figure 2.9).

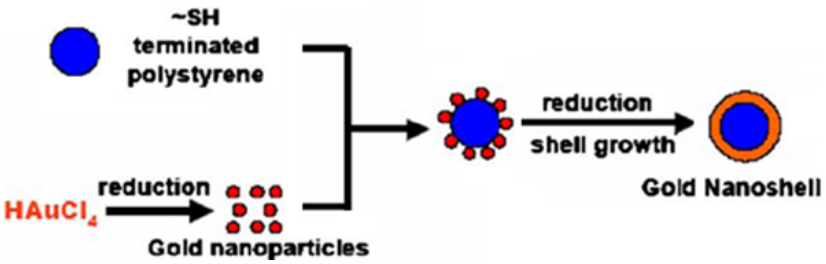

Figure 2.9 Schematic illustration of the synthesis of gold nanoshells [32].

The unique property of the Au nanoshells is that an dielectric void and a metallic Au shell could give a tunable surface plasmon resonance in a broad range of the spectrum (visible to near-infrared) [33, 34]. The thickness of shell rules the scattering and absorbing properties of the nanoparticles (Figure 2.10) [35]. When the SPR peaks of Au nanostructures are set within the near-infrared region, they can be used as “transparent window” for soft tissues contrast agents in bioimaging. The potential applications include surface enhanced Raman scattering (SERS) [36-39] and bioimaging contrast enhancement [6, 40-42].

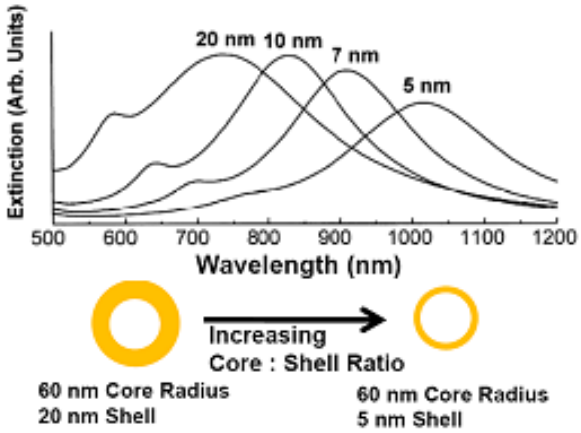

Figure 2.10 Theoretically calculated optical resonances of metal nanoshells silica sore, Au shell [35].

2.2 Electrolytes for Au Electrodeposition

For gold salt electrolytes, Au ions can be combined with different complexes which are mainly classified into cyanide and non-cyanide complex. The gold(I) cyanide complex $[Au(CN)_2]$ is one of the most important gold salt electrolytes for electrochemically deposition used in acidic, neutral or alkaline condition because of its high stability. However, there are several shortcomings for using $[Au(CN)_2]$ in acid such as toxicity and disposal concerns. Thus many non-cyanide systems have been developed [43-45].

Non-cyanide baths could be operated in mild acid with stabilizing additives by either electrolytic or electroless mechanism. Sulfite bath is the commonly used complex for cyanide free electrolyte, but the main problem with the sulfite system is the lack of stability with gold complexes. For a homogenous reversible reaction, the law of mass-action dictates that

$$\frac{[Au(I)-complex]}{[Au][complex]} = \beta\ (constant) \tag{2.3}$$

where [Au], [complex] and [Au(I) - complex] are the concentration of gold ion, complex ion and gold complex, respectively, in the solution. The constant, β, is a measurement of the strength of the complexant. Since the disproportionation of gold in solution is controlled by the concentration of gold complex, the stability constant for the complex is the determination of the bath stability. In the sulfite bath, gold presents in form of $[Au(SO_3)_2]^{3-}$ which suffers from instability at pH < 8. The stability constant of sulfite complex is approximately 10^{10} (Equation 2.4), the magnitude of which is several orders smaller than that of cyanide complex which is roughly 10^{38} (Equation 2.5) [46, 47].

$$[Au^+] = \frac{[Au(CN)^-_2]}{[CN^-_2]} * 10^{-38} \tag{2.4}$$

$$[Au^+] = \frac{[Au(SO_3)_2{}^{3-}]}{[SO_3{}^{2-}]^2} * 10^{-10} \tag{2.5}$$

Discharge of the gold(I) sulfite complex goes through the following three steps [48].

$$Na_3Au(SO_3)_2 \rightarrow 3Na^+ + Au(SO_3)_2^{3-} \quad (2.6)$$

$$Au(SO_3)_2^{3-} \rightarrow AuSO_3^{2-} + SO_3^{2-} \quad (2.7)$$

$$AuSO_3^- + e \rightarrow Au + SO_3^{2-} \quad (2.8)$$

Due to the low stability of Au (I) sulfite complex, gold(I) ions causes a disproportionation reaction (Equation 2.9) when they are operated under pH 8. [48-50]

$$3Au^+ \rightarrow 2Au^0 + Au^{3+} \quad (2.9)$$

Metallic gold and gold (III) ions are formed in the solution which becomes turbid as a result of colloidal precipitation and finally decomposes. This spontaneous decomposition issue of the bath had been tackled by adding stabilizing additives to enhance the stability.

Many approaches have been presented to enhance the stability of sulfite baths. H. Honma [48, 50] presented a gold(I) sulfite bath operable at pH 8 using 2,2`-bipyridine as stabilizing additives. These agents inhibit the disproportionation of Au^+ and greatly improved the bath stability. Morrissey [51] has developed a gold(I) sulfite bath which is stable from pH 4.0 to pH 6.5 using polyamines and aromatic nitro compounds as additives. These stabilizers suppress the disproportionation reaction to a large extent presumably through the formation of its complex with Au^+.

Other types of bathes were demonstrated having higher stability without stabilizer. Ammonium sulfite baths have also been developed which are operable in the pH range 6 - 8. The slightly acidic electrolytes containing tri-ammonium citrate, $KAuCl_4$ and Na_2SO_3 have been utilized as the stable gold solution. These electrolytes appear to be stable in the absence of stabilizing additives, and yet have not found wide use due to the low quality of gold [52, 53]. The mixed ligand electrolyte, sulfite-thiosulfate baths, without additives have been demonstrated and characterized to be stable with a pH close to 7.0 [49, 54-56]. The formation of colloidal gold can be avoided by combining Au(I) with thiosulfate (stability constant = 10^{26}), and sulfite prevents the formation of sulfur by maintaining a high level of bisulfite (HSO_3^-) in the solution [44, 56].

However, the baths were found to be unstable at neutral or slightly acid condition due to the disproportionation of free thiosulfate ions in forming colloidal sulfur as shown in Equation 2.10, and that of sulfite ions in forming SO_2 [45, 49, 56]:

$$S_2O_3^{2-} \leftrightarrow S + SO_3^{2-} \quad (2.10)$$

The summary of gold electrodepostion electrolytes is given in table 2.1.

Table 2.1 Summary of Gold Electrodepostion Electrolytes

Bath	***Cyanide***	***Sulfite***	***Ammonium Sulfite***	***Sulfite-thiosulfate***
Stability	High	Low	Medium	Medium
Stabilizer	N	EDA	N	N
Stable at pH	6~10	5 - 8	6 - 8	Near neutral
Toxicity	Y	N	N	N

In this study, the gold(I) sulfite bath was applied, and stability of which was improved by ethylenediamine (EDA), a sort of organic amine, working as the stabilizing additive. The ligand complexes of EDA with free Au^+ ions can suppress the disproportionation reaction. Therefore, EDA would be able to stabilize the electrolytes and enable operation of gold(I) sulfite bath within pH ranger of 5 - 8 [44, 50].

2.3 Nanobubbles at Solid/Liquid Interface

Small bubbles of gas exist at the interface between hydrophobic solids and water has been observed in the past decade. Scientists are puzzled by the nanobubbles that can develop on solid surfaces under liquid. The existence of nanobubbles has not been unequivocally established for following reasons. Firstly, the total free energy of a system in which water is in contact with a hydrophobic surface always promotes the formation of a gas layer unless the surface is extremely rough. Secondly bubbles in nanoscale would dissolve and disappear rapidly because of high internal pressure associated with the interfacial curvature thus resulting in the increase of gas solubility [57]. It is still not understood why these bubbles can remain

stable for hours. They are something of a mystery, but it is possible to generate these nanobubbles [58-67].

In bubble nucleation, gas may first be trapped at surface sites on a solid surface. Further diffusion of dissolved gas from bulk solution would then enlarge the bubble, a process related to the solid surface hydrophobicity, as well as the level of gas supersaturation. During wetting of a hydrophobic surface with a polar solvent, spherical cap bubbles with dimensions of 5 – 100nm in height and 0.1 - 0.8μm in diameter are produced [60, 65, 66]. Theoretical studies and experimental studies suggest that at the liquid-solid interface, the presence of nanobubbles is responsible for the apparent slip or the breakdown of the no-slip condition for hydrophobic surfaces.

The existence of nanobubbles at the solid-liquid interface has been detected by various techniques, such as atomic force microscopy (AFM) [59, 65, 68], rapid cryofixation/freeze fracture [69], neutron reflectometry [70] and infrared spectroscopy [71]. AFM has been using as a powerful tool for detecting small bubbles due to morphological characterization and force detection on the nanoscale. In high-resolution tapping-mode atomic force microscopy (TMAFM), an oscillating tip is brought to be intermittently in contact with the sample surface by applying a lighter force compared with that applied in contact mode AFM. Thus, the technique is commonly used to detect nanobubbles. As for liquid, highly purified water is mainly used as medium in some of the experiments, though others could have been done with alcohols or diluted sulfuric acid solutions.

It has also been demonstrated that nanobubble could form even on hydrophilic surface. Hu and co-workers also showed that small bubbles less than 100nm in diameter could form on both hydrophobic (HOPG) and hydrophilic (freshly cleaved mica) surfaces [61]. Nanobubbles were prepared on the smooth and hydrophilic mica surface by the exchange of ethanol and water and imaged with TMAFM in fluid. The gas dissolved in the liquids was essential for the formation of nanobubbles at the mica/water interface. Ishida [72] used the silicon wafer surface

which was hydrophobized by silanation with octadecyltrichlorosilane (OTS) to observe the surface in-situ by TMAFM after immersing wafer into water. The small bubbles with a base diameter of 10 – 50nm on the hydrophobic substrate surface were found.

The measured physical properties of these nanobubbles are found to be comparable to those of macroscopic bubbles in all respects other than the contact angle. The contact angle of nanobubbles was found to be much larger than the macroscopic contact angle on the same substrate. The larger contact angle results in a larger radius of curvature and a commensurate decrease in the Laplace pressure. The addition of surfactant increases the compliance of the interface causing the accompanying decrease in surface tension. Youngsuk [73] reported a surprising consistent finding where indicated that the apparent contact angles of nanobubbles could exceed 160°.

Since electrochemical reactions occur primarily in aqueous solutions, gases (hydrogen and oxygen) are usually generated at electrode surfaces. Accordingly, electrochemical generated gases may form nanobubbles and attach to the electrode surface. This phenomenon in return significantly affects the electrochemical reaction system. Zhang [74] presented the electrochemically controlled formation of hydrogen nanobubbles on bare HOPG surface via TMAFM (Figure 2.11). Moreover, the formation and growth of nanobubbles could be controlled by tuning either the applied voltage or the reaction time. The evolution process of nanobubbles can be described as formation, growth, coalescence, as well as the eventual release of merged microbubbles from the HOPG.

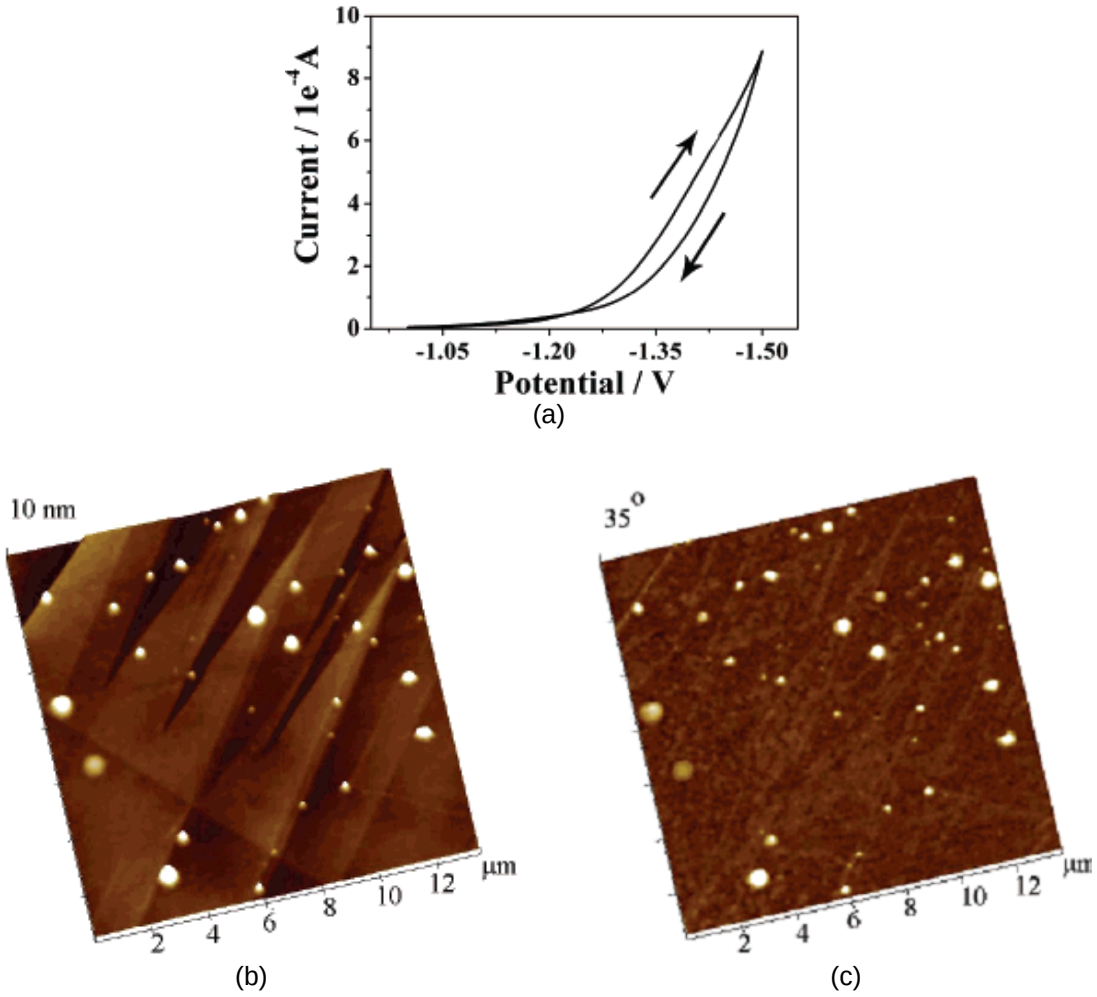

Figure 2.11 (a) cyclic voltammetry curve of 0.01M H_2SO_4 at a scan rate 0.2V/s, hydrogen evolution begins at approximately -1.2V; AFM images of (b) height and (c) phase images of electrochemically generated nanobubbles on HOPG surface at voltage -1.5V for 10s [74].

The presence of nanobubbles controlled by using nanopatterned surfaces has been demonstrated [68]. Nanoscale domains with various hydrophobicities which give birth to periodically ranged arrays of hydrophobic and hydrophilic domains were used with the purpose of produce the formation and extent of nanobubbles. In addition to the control of surface hydrophobicity, it is important to keep the spatial dimensions of the hydrophobic domains consistent with the equilibrium topology of the nanobubbles. By using heterogeneous surfaces

with controlled chemical treatment and lateral size, the location and number density of nanobubbles can be systematically controlled.

2.4 Electroless Deposition

The formation of hollow Au nanoparticles includes electrochemically evolved hydrogen nanobubbles and electroless reactions. Electroless deposition is the spontaneous reduction and oxidation of metal ions in an aqueous solution form metallic particles or films in the absence of an external source of electric current [43, 75, 76]. Electroless deposition is usable to a wide range of substrate combinations, including metal-metal, metal-semiconductor, and metal-insulator. This is important with regard to metal deposition on isolated substrate regions. The literature commonly classifies “electroless deposition” into three fundamentally different mechanisms (Figure 2.12) [49, 77]. These include autocatalytic, substrate catalyzed, and galvanic displacement processes.

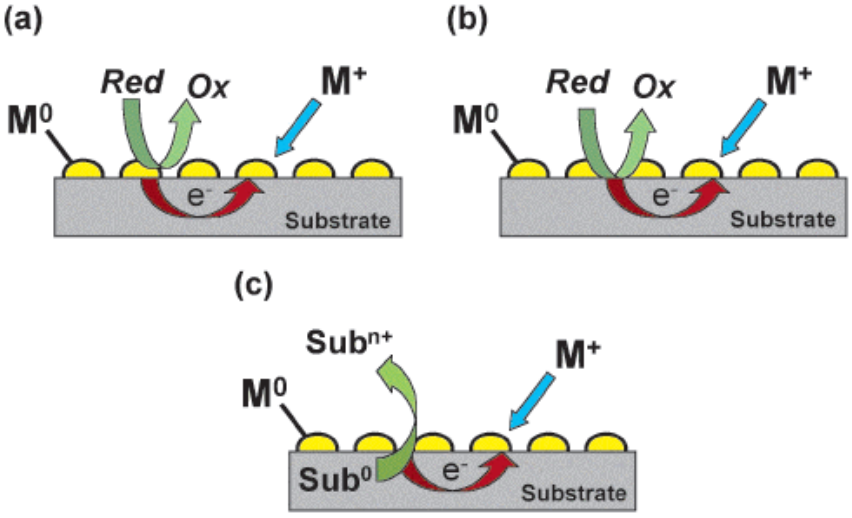

Figure 2.12 Electroless deposition processes: (a) autocatalytic: the reduced noble metal serves as the catalyst for further reduction of the metal salt by the external reducing agent; (b) substrate catalyzed: the substrate surface catalyzes the reduction of the metal salt by the reducing agent; (c) Galvanic displacement: the surface serves as the reducing agent and electron source for reduction of the metal salt [77].

Autocatalytic process uses a complex electrolyte composition to allow the reduced metal itself to serve as a catalyst for further reductive deposition. Once initiated, the reduced

metal species serve to catalyze subsequent metal reduction. In autocatalytic system, the electrolytes typically contain a metal salt, a pH adjuster, a reducing agent, and other various additives. Similarly, substrate catalyzed deposition baths also contain a metal salt and reducing agent, but metal reduction is facilitated on the substrate surface. Once the surface is completely covered, metal ions cease to be reduced from solutions because the surface is no longer exposed [43, 78].

In the case of galvanic displacement, the process is in an entirely different manner. The deposition is carried out in the absence of an external reducing agent [49] because the reducing electrons are provided by the substrate itself. The reducing electrons are derived from the valence band or bonding electrons of the solid and reduce metal ions in solution to metallic particles on the surface [79] . Deposition proceeds as long as oxidized substrate ions are able to permeate through the metal film into solution, or until a dielectric layer of oxidized substrate forms, thereby, halting electron transfer.

CHAPTER 3

EXPERIMENTS

3.1 Preparation of Electrolytes

The electrolytes for electrodeposition were prepared with reagent-grade chemicals and high purity water produced from a Millipore Milli-Q water purification system. Gold(I) cyanide solution (pH ~ 7) and commercially available gold(I) sulfite solution (TECH-GOLD 25 ES RTU) (pH ~ 6.8) were purchased from VWR and TECHNIC Inc. without any further modification. The composition of the commercial gold(I) sulfite solution consists of 2 - 5% sulfuric acid, 2 - 5% ethylenediamine, <10% sodium gold(I) sulfite and 5 - 10% sodium sulfite. The pure sodium gold(I) sulfite solution ($(Na_3Au(SO_3)_2$ pH ~ 10.5) was purchased from Colonial Metals Inc. diluted to 10% with deionized water. 99% of ethylenediamine (EDA) was diluted to 50% with deionized water used as a stabilizing additive to suppress the disproportionation of Au(I)-sulfite complex. 0.4M of Ni sulfate hexahydrate and Ni sulfamate tetrahydrate were prepared by adding 12.4g of Ni sulfate and 26g of Ni sulfamate into 200ml deionized water respectively. Except gold(I) cyanide solution, all other baths were acidified to pH ~ 6 with a 5% of sulfuric acid solution. All chemicals were prepared in room temperature.

Several of chemical solutions which were used for understanding the reduction of Au ions from electrochemically evolved hydrogen bubble are given in Table 3.1. Gold(I) cyanide, commercial gold(I) sulfite and diluted $Na_3Au(SO_3)_2$ electrolytes were used to study the electrochemical behaviors of bathes. Self-prepared gold(I) sulfite solution with the addition of stabilizer (EDA) was used to understand the stability of electrolytes. Ni sulfate hexahydrate and Ni sulfamate tetrahydrate were used out to investigate the effects of Ni^{2+} ions on hydrogen evolution efficiency. The self-prepared solutions with other addition chemicals were mixed in the

following order: Diluted $Na_3Au(SO_3)_2$ → EDA → 0.4M of Ni sulfate/sulfamate → 5% of sulfuric acid (if the chemical is applied).

Table 3.1 Summary of Gold Electrolytes Composition

Additives / ***Bath***	*EDA*	*Ni Sulfamate*	*Ni Sulfate*	*Acidifier*	*pH*
Commercial Gold(I) Cyanide					**~6.8**
Commercial Gold(I) Sulfite				**¥**	**~6**
Commercial Gold(I) Sulfite		**¥**			**~6**
Self-Prepared Gold(I) Sulfite				**¥**	**~6**
Self-Prepared Gold(I) Sulfite	**¥**			**¥**	**~6**
Self-Prepared Gold(I) Sulfite		**¥**		**¥**	**~6**
Self-Prepared Gold(I) Sulfite	**¥**	**¥**		**¥**	**~6**
Self-Prepared Gold(I) Sulfite			**¥**	**¥**	**~6**
Self-Prepared Gold(I) Sulfite	**¥**		**¥**	**¥**	**~6**

3.2 Preparation of Substrates

Different kinds of substrates including silicon wafer, glass and Anodic Alumina oxide (AAO), were employed in the experiments. Oxidized silicon wafer with 1μm thickness of SiO_2 has been chosen as a substrate for this work because of the low conductivity of SiO_2 (1×10^{13} Ω·m at 20° C). The wafer was cleaned using organic solvents under ultrasonication for 20 minutes. Rinsed with deionized wafer, the wafer was then dried with nitrogen gas. The glass substrate was taken from plain microscope slides purchased from VWR. The glass was rinsed with deionized water and cleaned by plasma treatment before use. Glass was chosen as a substrate due to the extremely low conductivity, and hydrophobicity which is similar to that of silicon wafer. The porous alumina membranes (Figure 3.1) were produced by electrochemical anodic oxidation of aluminum film on silicon wafer. The process was conducted in a typical two-

electrode cell with platinum mesh as the counter electrode at 40 volts. 0.23M of oxalic acid was used as electrolytes at 4 - 10˚C. The pores of alumina membranes were enlarged by acid treatment (10% of H_3PO_4).

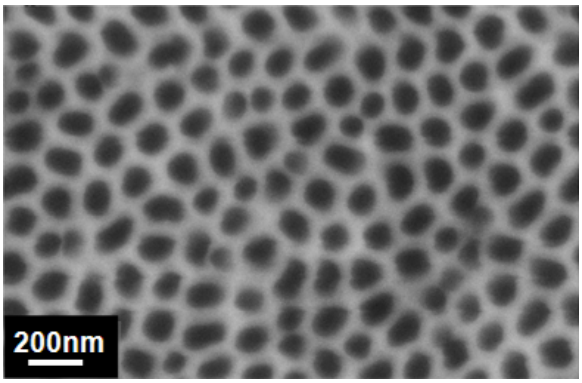

Figure 3.1 Enlarged porous alumina membranes.

The photolithography technique was use for patterned substrate. The design of photomask used in the experiments is shown in Figure 3.2a. The width of the stripes is 50µm, and the stripes were duplicated every 100µm. The Ag strip patterned substrate is shown in Figure 3.2b.

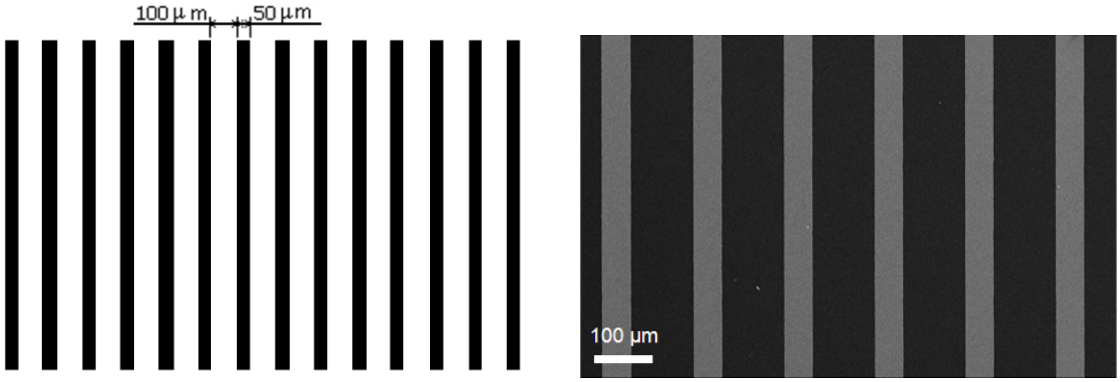

(a) (b)

Figure 3.2 (a) Mask pattern for photolithography; (b) Ag striped pattern substrate.

In addition, the substrate was first heated up to 105˚C for one minute to remove mist. Hexamethyldisilazane (HMDS), an adhesive used for spin, was spin casted on the substrates.

On the top of which, photoresist AZ5214 was then spin casted using Headway Spinner (Figure 3.3a) at 4500 rpm for 30 seconds. The prebake process for the substrates was carried out at 105˚C for 60 seconds in order to evaporate solvent before the exposure of the substrate to UV light. The contact aligner, MJB3 Karl Suss Mask Alinger (Figure 3.3b), was used in photolithography process.

(a) (b)

Figure 3.3 (a) Headway Spinner; (b) MJB3 Karl Suss Mask Alinger.

The elements of a typical contact aligner are shown in Figure 3.4 [80]. The substrate was exposed to UV light (mercury lamp 279 Watt) for 9 seconds to activate the photoresist. In the next step, the sample was heated up to and kept at 130˚C for 60 seconds to crosslink the activated photoresist. The crosslinked photoresist became insoluble in developer and no longer light sensitive, while the behavior of the unexposed part of photoresist did not change. After a 45 seconds period of flood exposure (no mask required), the unexposed areas were dissolved in the developer, AZ327 MIF, while the crosslinked areas remained. The overall process resulted in a negative image of the mask pattern.

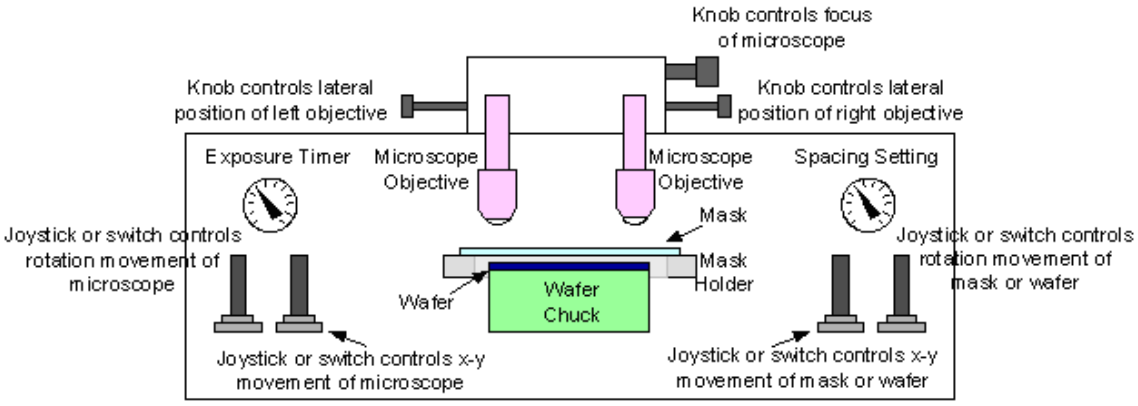

Figure 3.4 Elements of a typical contact aligner [80].

3.3 Electrode and Thin Film Deposition

The deposition of the desired metal electrode on substrates was conducted using the thermal evaporator (NRC 3117) (Figure 3.5). The chamber was first vacuumed by the mechanical pump to 10^{-3} Torr. After that, the cryo pump (T < 15 K) was used to vacuum the chamber from 10^{-3} to 10^{-6} Torr. Once the chamber reached ideal deposition temperature, a 15nm-thick layer of Cr was first deposited on the substrate to improve the adhesion of desired metal layer which was then deposited on the top of Cr layer with a thickness of 150nm. The thickness was indicated by quartz-crystal balance inside chamber. The non-patterned substrate was ready to use in this stage. For patterned substrate, lift off technique was used to remove photoresist. In order to do that, the substrate was placed in acetone under ultrasonication for 30 seconds, resulting in the striped electrode.

Figure 3.5 Thermal evaporator used for desired metals deposition to fabricate the working electrode.

3.4 Electrodeposition and Cyclic Voltammetry

The electrodeposition experiments were conducted by using a typical three-electrode cell with Ag/AgCl (sat KCl) reference electrode in 3M NaCl solution and platinum mesh (surface area 1.26 cm^2) as the counter electrode at room temperature (Figure 3.6). All potentials are quoted versus Ag/AgCl (sat KCl.) Different materials of substrates were applied as a working electrode. The resistance between substrate and working electrode was smaller than 0.8 Ω. The experiments were performed under various potentials controlled by a potentiostat (Princeton Applied Research 273A) (Figure 3.7.)

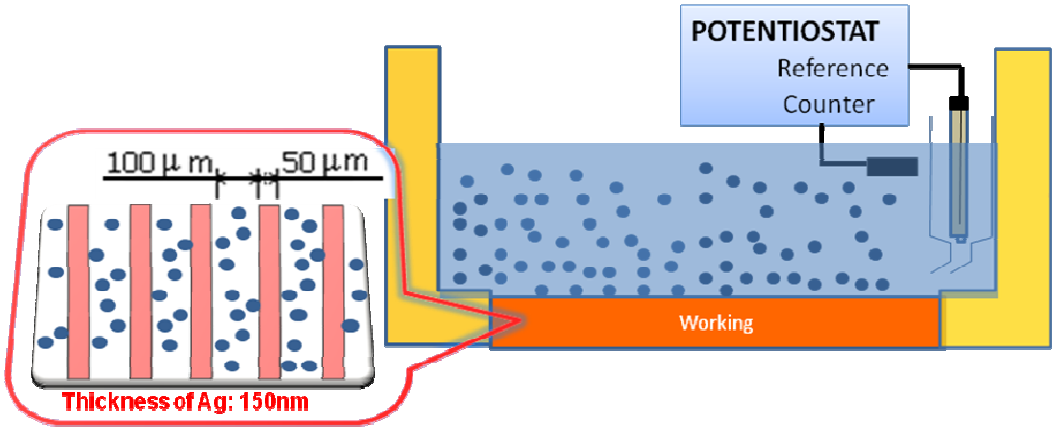

Figure 3.6 Three-electrode cell setup.

Figure 3.7 Potentiostat (Princeton Applied Research 273A) for electrochemically deposition.

Cyclic voltammetric measurements were carried out in the conventional three-electrode system using potentiostat (Princeton Applied Research 273A.) The working electrode was Au film which deposited on silicon wafer. All electrolytes were adjusted with H_2SO_4 to pH 6, except the gold(I) cyanide electrolyte due to the toxicity concern. The equipment setup is the same as the electrodeposition. A stable open circuit potential was reached before cyclic voltammetry experiments. The voltage was scanned with sweep rate at $5mVs^{-1}$ starting from an open circuit potential to negative direction.

3.5 Characterization

Various characterization tools were employed to investigate the hollow Au nanoparticles including ion milling (Figure 3.8a), scanning electron microscope (SEM) (Figure 3.8b), energy dispersive X-ray spectrophotometer (EDS) and high-resolution transmission electron microscopy (HRTEM) (Figure 3.8c).

In order to reveal the cross section of hollow Au nanoparticles, a stirrer was used to separate the particles into the electrolytes during synthesis process. The particles were collected, cleaned with deionized water and placed on the surface of silicon wafer. Particles were then treated by ion milling with switching beam mode at 4˚, 4.5 keV for 2 minutes.

SEM was applied to characterize the formation, morphology, size distribution of the nanoparticles. Energy dispersive X-ray analysis (EDAX) was used for analyzing the elements. High-resolution transmission electron microscopy (HRTEM) was employed to capture the shell structure of the particles.

(a)

(b)

(c)

Figure 3.8 (a) Gatan model 691 precise ion polishing systems (PIPS); (b) ZEISS Supra 55 VP scanning electron microscope (SEM); (c) H-9500 High-resolution transmission electron microscopy Hitachi (HRTEM).

CHAPTER 4

RESULTS AND DISSCUSION

4.1 Electrochemical Properties of Au Electrodeposition Electrolyte

Cyclic voltammetry (CV) was first carried out in this project to study the electrochemical behaviors and reduction potentials of the different gold electrolytes. The investigated electrolytes include sodium sulfite (Na_2SO_3), self-prepared gold(I) sulfite $Na_3Au(SO_3)_2$ with and without EDA and commercial gold(I) sulfite (Au 25 ES RTU). The CV measurements were recorded starting from open circuit potential toward the negative direction. Figure 4.1 shows the reduction potential of different electrolytes. All solutions have a pH of 6.0..

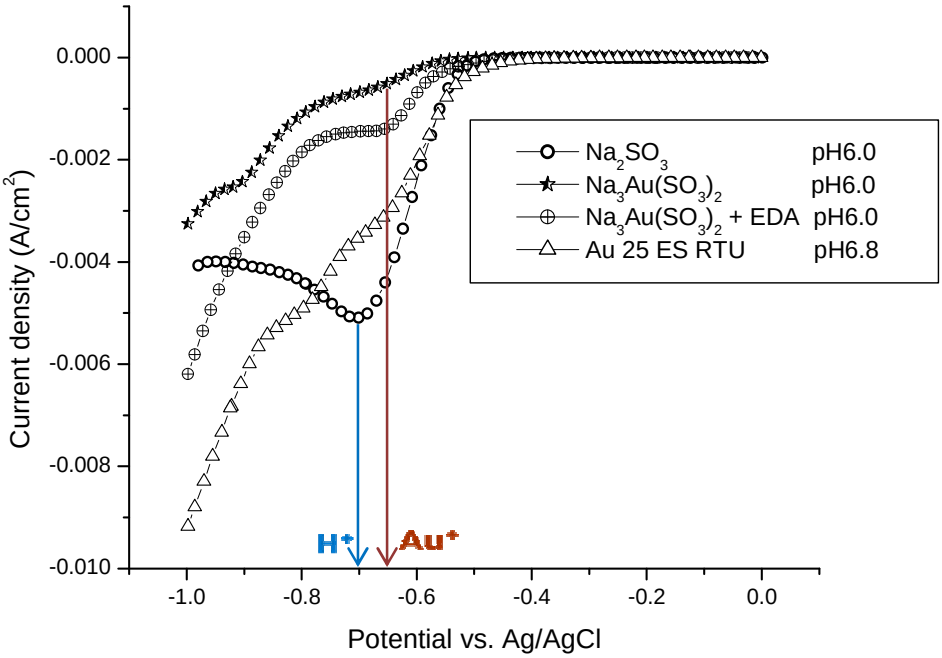

Figure 4.1 Cyclic voltammograms for various electrolytes from open circuit potential to 1.0V at scan rate $5mVs^{-1}$.

The CV measurement of the Na_2SO_3 electrolytes indicates that the reduction peak of H^+ was at potential -0.7V (versus Ag/AgCl). For self-prepared gold(I) sulfite electrolytes, the reduction potential of Au^+ was observed around, -0.65V. The current increased at more negative potential was due to the hydrogen evolution reaction.

The CV measurement shows that the electrochemical behaviors of the self-prepared gold(I) sulfite electrolytes with/ without EDA were very similar. The reduction potential of Au^+ has appeared at the same potential (-0.65 V). The CV curve of commercial gold(I) sulfite solution which contains EDA, shows the same reduction potential of Au^+ as gold(I) sulfite solution. For these three different gold(I) sulfite solutions, the reduction potential of Au^+ all lies in -0.65V, the differences are the hydrogen evolution potential and current density.

4.2 Observation of Au Nanoparticle Formation on Non-Conductive Substrate

In order to study the formation of Au nanoparticles, a glass substrate patterned with periodical Ag strips was used as working electrode in Au electrochemical deposition. The metal strips served as working electrode, and non-conductive areas were used to observe the electroless deposition.

When the applied potential was more negative than -0.6V, we observed a large amount of Au nanoparticles formed on the non-conductive areas, as shown in Figure 4.2. When the potential is more positive than -0.6V, only Au deposition occurred on the surface of Ag strips, and no particles were observed on the non-conductive areas. Using the Nernst equation, we calculated the hydrogen evolution potential, which is -0.55V at pH 6. Electroless deposited Au nanoparticles have only been observed when the applied potential is more negative than hydrogen evolution potential. This strongly suggests that hydrogen evolution is involved in the formation of Au nanoparticles.

According to the principles of electrodeposition, materials can only be deposited on conductive electrode surfaces; in the other words, electrochemical deposited Au nanoparticles

cannot exist on the non-conductive areas. The possible reason for the formation of Au nanoparticles on the non-conductive areas is electroless deposition.

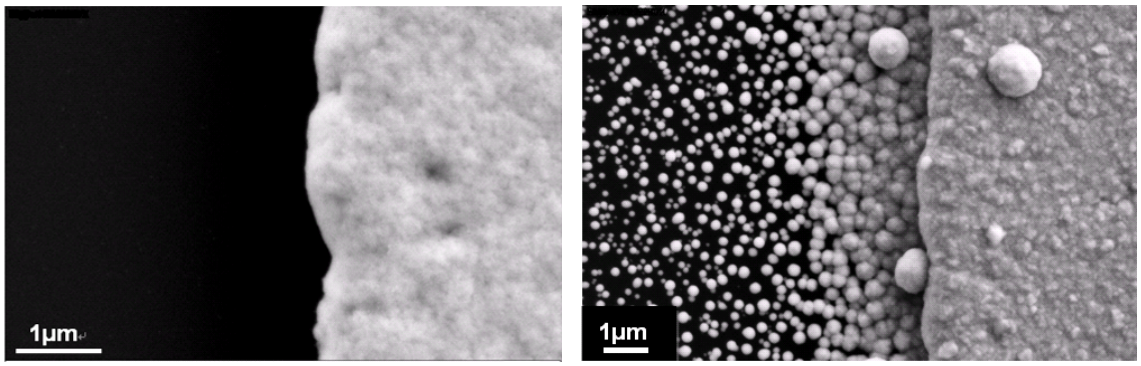

(a) (b)

Figure 4.2 SEM micrographs of formation of Au nanoparticles on non-conductive substrates patterned with periodical Ag strips at applied potential: (a) -0.5V; (b) -0.6V.

In order to exclude the possibility of the Au nanoparticles formation from the edge of the metal strips, we compared two electrolytes, gold(I) sulfite and gold(I) cyanide, at potential -0.8V. As shown in Figure 4.3, only using the gold(I) sulfite electrolytes, Au nanoparticles can form on the non-conductive areas. Using gold(I) cyanide electrolytes, no Au nanoparticles were formed on the non-conductive areas, but only a thin film of Au formed on the metal strips.

All results above strongly suggest that electroless deposition and hydrogen evolution play critical roles in the formation of Au nanoparticles in gold(I) sulfite electrolytes.

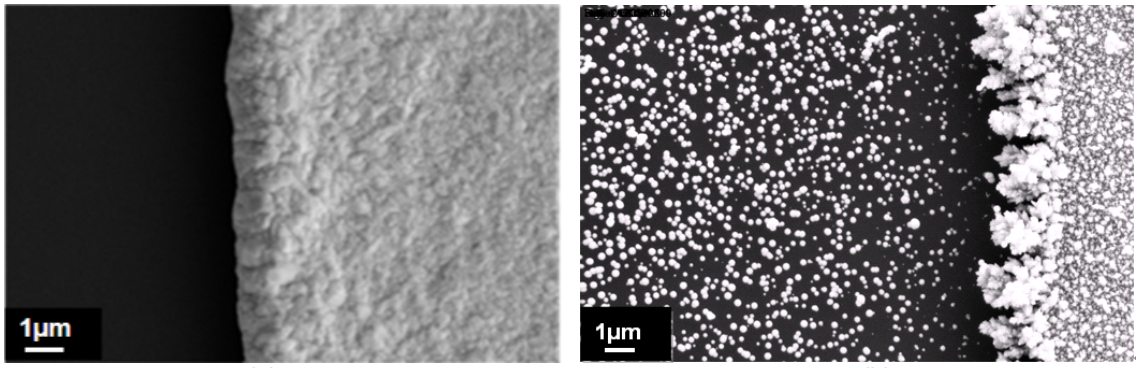

(a) (b)

Figure 4.3 SEM micrographs of Au nanoparticles formation from: (a) gold(I) cyanide electrolytes; (b) gold(I) sulfite electrolytes on patterned substrates at potential -0.8V.

4.3 Effect of Different Parameters on Au Nanoparticle Formation

In this section, the effects of stabilizer, additive, potential, and hydrophobicity of substrate were investigated. Pure gold(I) sulfite solution ($Na_3Au(SO_3)_2$) had been diluted into self-prepared gold(I) sulfite solution, and modified by adding additives. Various substrates with different hydrophobicities were used.

4.3.1 Effects of EDA

In the commercial gold(I) sulfite electrolytes, which we have used for above mentioned experiments, Ethylenediamine (EDA) is added as a stabilizer. To study the effects of EDA on Au nanoparticle formation, we prepared gold(I) sulfite electrolytes in the absence of EDA. Figure 4.4 shows the SEM micrographs using electrolyte with and without EDA. No well-defined Au nanoparticles formed when the electrolytes without EDA were used. Few small irregular Au particles on the non-conductive areas were formed. We believe that they were from disproportionation reaction due to the low stability of the electrolytes when the pH of the electrolytes is lower than 8.

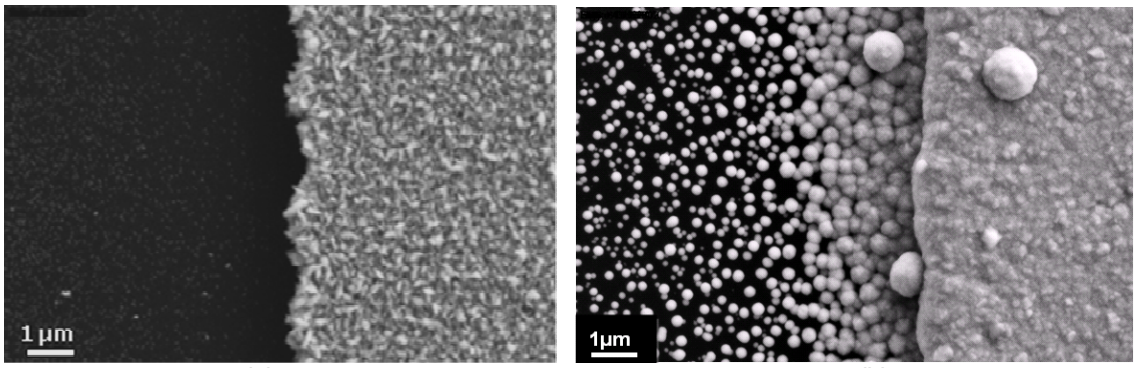

(a) (b)

Figure 4.4 SEM micrographs of Au nanoparticles from self-prepared gold(I) sulfite electrolytes; (a) in the absence of EDA; (b) in the presence of EDA, on patterned substrates.

To confirm that the participated Au can form from disproportionation reaction in the electrolytes, a silicon wafer which has very poor conductivity was used as the substrate immersed into the same condition of the electrolytes through electroless deposition for the same

period of the electrodeposition time. As expected, the precipitated Au was also obtained from electrochemical deposition and electroless deposition.

For electrolyte with EDA, it clearly shows Au nanoparticles can be formed on the non-conductive areas. Using this electrolyte, we studied the nanoparticle formation at various applied potentials. Figure 4.5 shows that when the potential was more positive than -0.5V, Au nanoparticles did not form on the non-conductive areas, and only a thin layer of Au deposited on the conductive working electrodes. Lowering the potential to -0.6V, a large amount of Au nanoparticles was formed on the non-conductive areas. This again suggests that the nanoparticle formation is related to the electrochemical reaction. However, further lowering the potential to -0.8V, large size of Au particles with irregular shape was observed on the both non-conductive areas and metal strip. The increase of size may be due to the rapid hydrogen evolution at lower potential.

The above observations suggest that EDA plays an important role in the stability of the gold(I) sulfite electrolytes. The complexes of EDA bond with free Au ions to suppress the disproportionation reaction. Therefore, the gold(I) sulfite electrolytes are able to be used with a lower range of pH.

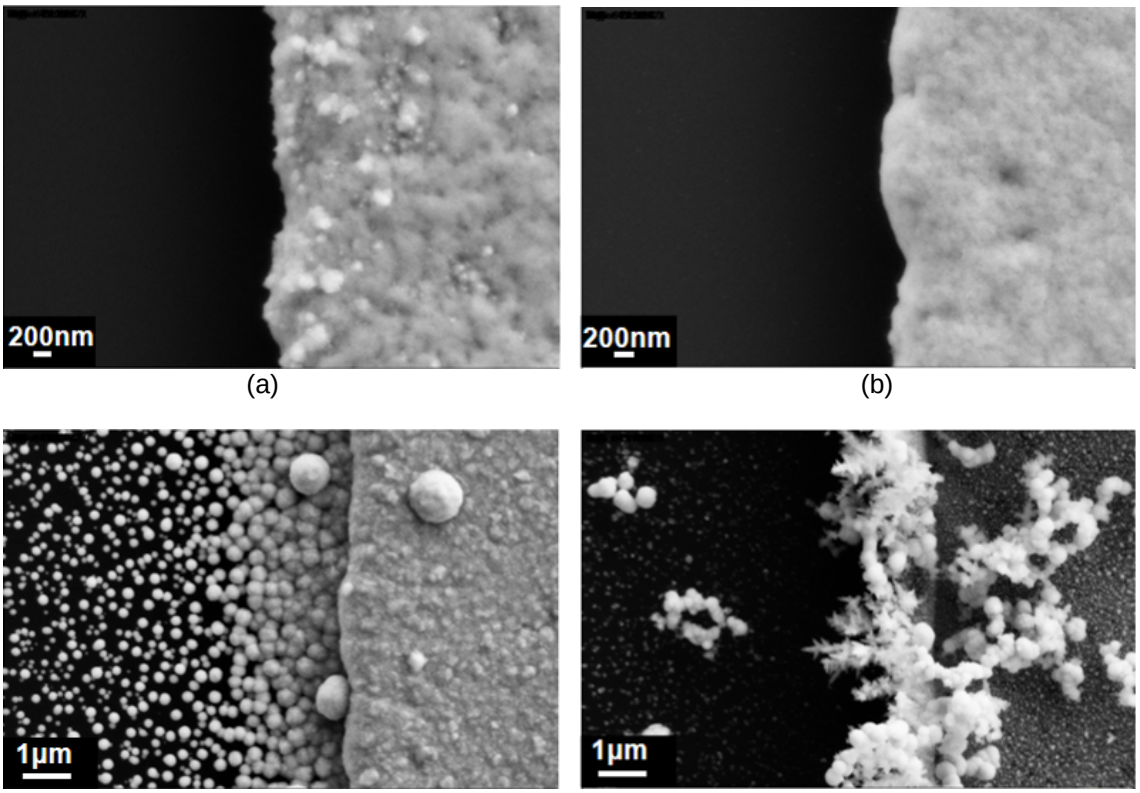

Figure 4.5 SEM micrographs of Au nanoparticles formation from self-prepared gold(I) sulfite electrolytes with the addition of EDA at potential: (a) -0.4V; (b) -0.5V; (c) -0.6V; (d) -0.8V.

Cyclic voltammetry (CV) was used to study the effects of EDA on the gold(I) sulfite electrolytes. The reduction potential of the gold(I) sulfite electrolytes with and without EDA were recorded starting from open circuit potential to -1.0V at the potential scan rate 5mV/s. The acidifier, sulfuric acid, is not believed to be a significant issue in these experiments. The CV measurement (Figure 4.6) shows that the current density of hydrogen evolution at potential -0.95V was increased from -2.8mA to -5.1mA after the addition of EDA. It seems that the addition of EDA greatly enhanced hydrogen evolution. A possible explanation for this enhancement is that EDA has the same function as ethylenediamine tetra acetic acid (EDTA) which has capability to clean removal of adhering surface oxides from active metal electrodes for hydrogen evolution (the Rowland effect) [81] [82-84].

The results show that the EDA, a key additive, was not only able to stabilize the gold(I) sulfite solutions, but also able to increase hydrogen evolution efficiency.

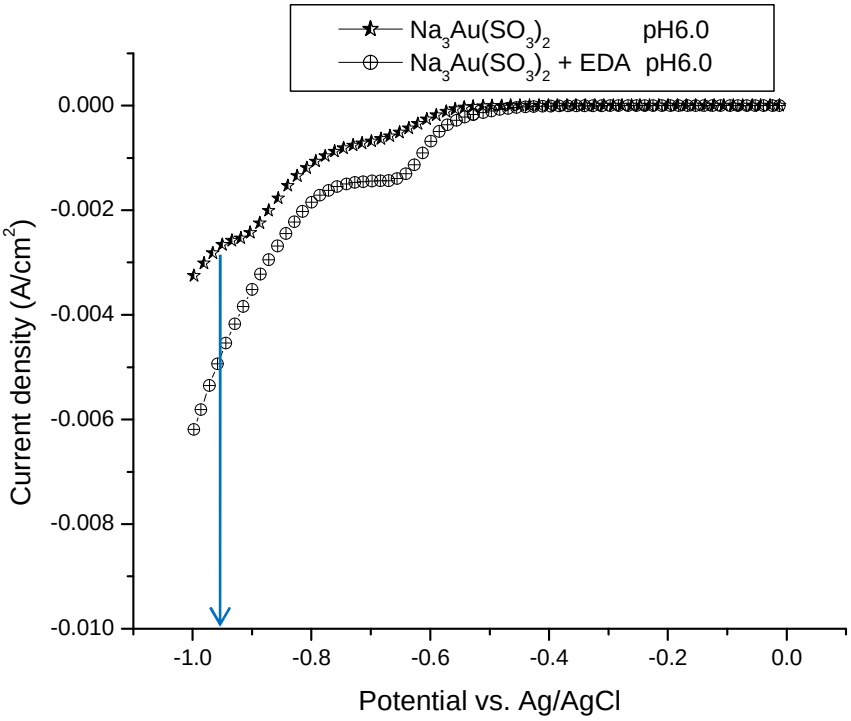

Figure 4.6 Cyclic voltammetry of self-prepared gold(I) sulfite electrolytes without/with EDA were recorded starting from open circuit potential to -1.0V at scan rate 5mVs^{-1}.

4.3.2 Effects of Ni^{2+} ion

The hydrogen evolution efficiency is directly associated with hydrogen exchange current density of metal electrodes. It is known that Ni metal has a relatively high current density in hydrogen evolution reaction. Therefore, Ni^{2+} ions were used as additive in the gold(I) sulfite electrolytes, aiming for enhancing the hydrogen evolution efficiency.

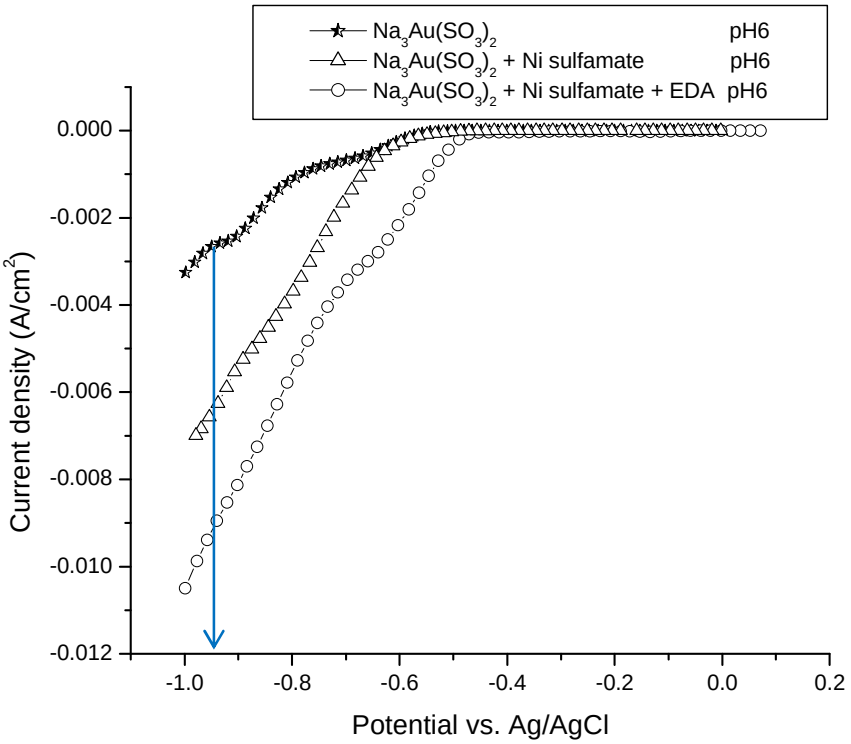

Figure 4.7 Cyclic voltammetry of self-prepared gold(I) sulfite electrolytes in the presence of Ni^{2+} ions without/with EDA were recorded starting from open circuit potential to -1.0V at scan rate $5mVs^{-1}$.

First, the hydrogen evolution efficiency was studied in the gold(I) sulfite electrolytes with and without Ni^{2+} ions by cyclic voltammetry. CV measurement (Figure 4.7) shows that the addition of Ni^{2+} ions and EDA greatly increased the hydrogen evolution efficiency. With Ni^{2+} ion, Ni metal gradually formed and replaced the electrode surface during the electrodeposition. The newly generated Ni metal has higher hydrogen exchange current density [85, 86]. Moreover, the addition of EDA can increase the hydrogen evolution efficiency as well. The current density of hydrogen evolution reaction at potential -0.95V (versus Ag/AgCl) was increased from -2.8mA to -6.5mA with the addition of Ni^{2+} ions and -9.2mA in the presence of both Ni^{2+} ions and EDA.

The effects of Ni^{2+} ions on Au nanoparticles were again investigated on non-conductive substrates patterned with Ag strips. Figure 4.8 shows Au nanoparticles formed from the gold(I)

sulfite electrolytes in the absence and presence of Ni^{2+} ions. It has been noticed that the size distribution of Au nanoparticles was greatly improved by the addition of Ni^{2+} ions. The improved size distribution of Au nanoparticles may be due to enhanced hydrogen evolution efficiency.

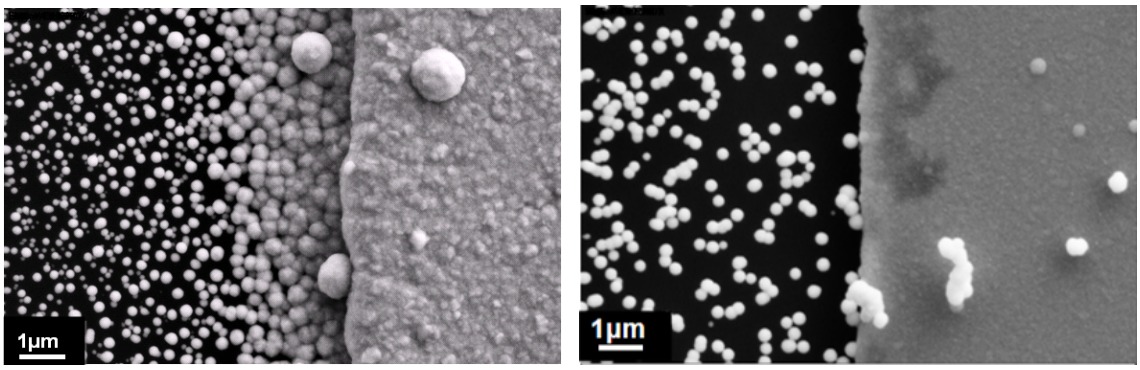

(a) (b)

Figure 4.8 SEM micrographs of Au nanoparticles formation from self-prepared gold(I) sulfite electrolytes with EDA: (a) in the absence of Ni^{2+} ions; (b) in the presence of Ni^{2+} ions at potential -0.8V on non-conductive substrates patterned with Ag strips.

The effects of Ni^{2+} ions on Au nanoparticles were also observed on plain conductive substrates. Figure 4.9 shows the electrochemically deposited Au from the gold(I) sulfite electrolytes in the absence and presence of Ni^{2+} ions. Without the addition of Ni, the deposited Au was very rough, but no well-defined particles formed. With Ni, a large amount of spherical particles appeared. Some parts of the spherical particles peeled off from the substrate to expose their interior. It clearly show hollow nature of these nanoparticles, which suggests that hydrogen bubbles act as templates for the formation of nanoparticles.

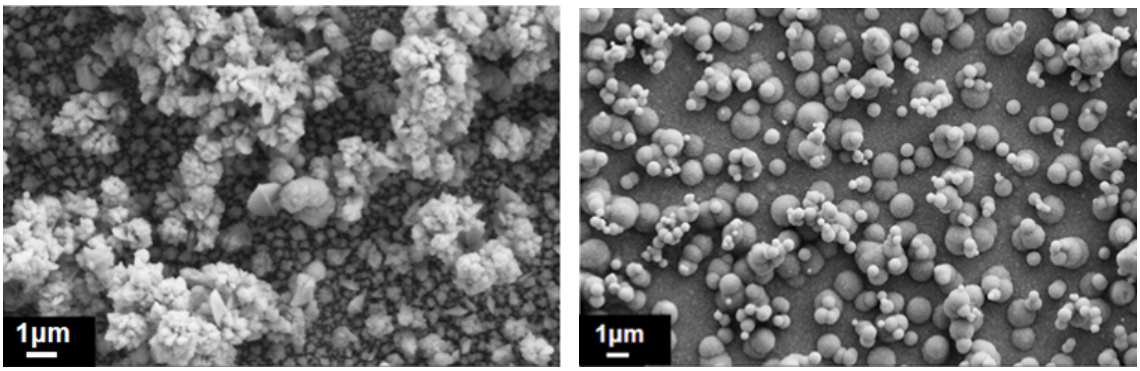

(a) (b)

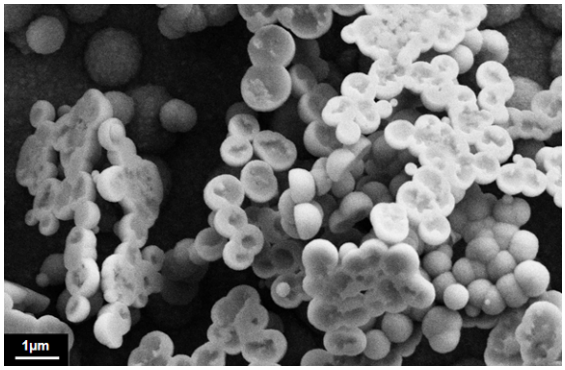

(c)

Figure 4.9 SEM micrographs of Au nanoparticles formation from self-prepared gold(I) sulfite electrolytes: (a) in the absence of Ni^{2+} ions; (b) in the presence of Ni^{2+} ions at potential -0.8V on conductive substrates on conductive substrates. (c) SEM micrographs showing bowl-shape Au nanoparticles released from the deposited thin film with bumps.

By stirring the electrolyte with a stirrer during the electrodeposition, the Au nanoparticles can be peeled off from the substrate into the electrolyte solution. Then the Au nanoparticles were collected from the solution and were cleaned by dispersing in DI water followed by centrifugation. The cleaned Au nanoparticles were placed on a Si wafer for EDS analysis (Figure 4.10b). It (Figure 4.11b) shows that Au nanoparticles are made of pure gold without Ni. EDS analysis (Figure 4.11a) of the electrodeposited thin film (Figure 4.10a) shows the film consists of Ni and Au. This indicates Ni and Au were electrochemically deposited, and Au nanoparticles were formed by electroless deposition.

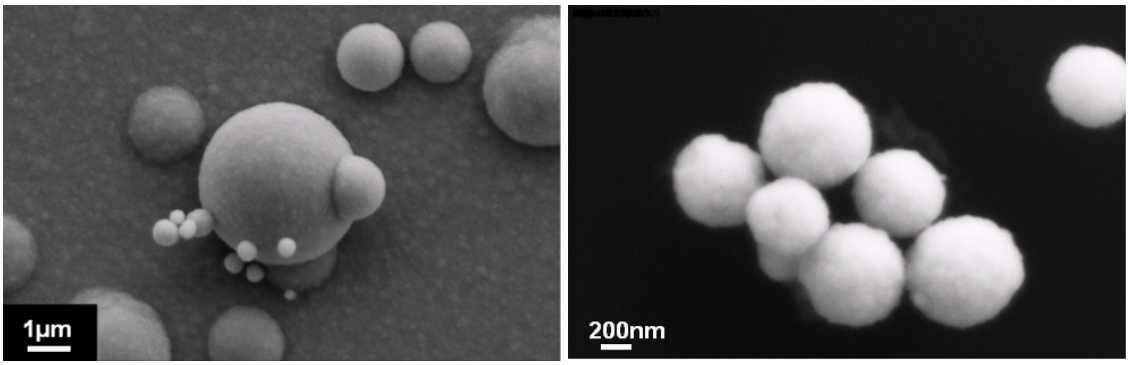

(a) (b)

Figure 4.10 SEM micrographs of: (a) electrochemically deposited thin film; (b) electroless deposited Au nanoparticles.

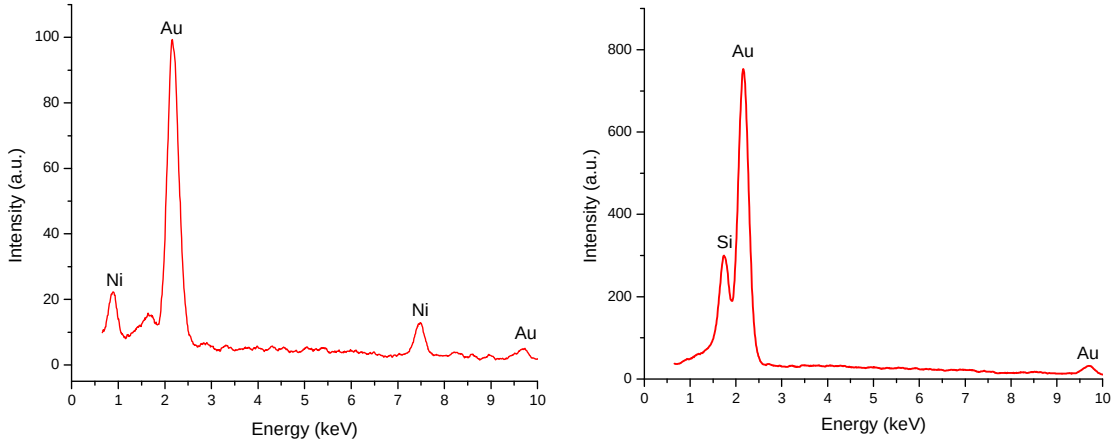

(a) (b)

Figure 4.11 EDS data of: (a) electrochemically deposited thin film; (b) electroless deposited Au nanoparticles.

The effects of Ni^{2+} ions on Au nanoparticles were further studied in the gold(I) electrolytes in the presence of Ni^{2+} ions at different potentials. Figure 4.12 shows no Au nanoparticles on the non-conductive areas at potential -0.4V. Lowering the potential to -0.5V and -0.6V, well-defined Au nanoparticles appeared on the non-conductive area. This is inconsistent with the assumption that hydrogen bubbles act as templates and reducing agents. However, when the applied potential was increased to -0.8V, no appearance of Au nanoparticles were observed, and the Ag strips were mostly covered by Ni instead of Au, as

shown in Figure 4.13. We speculated that the reduction of Ni ions was mainly discharged at this potential instead of hydrogen evolution, thus no Au particles formed.

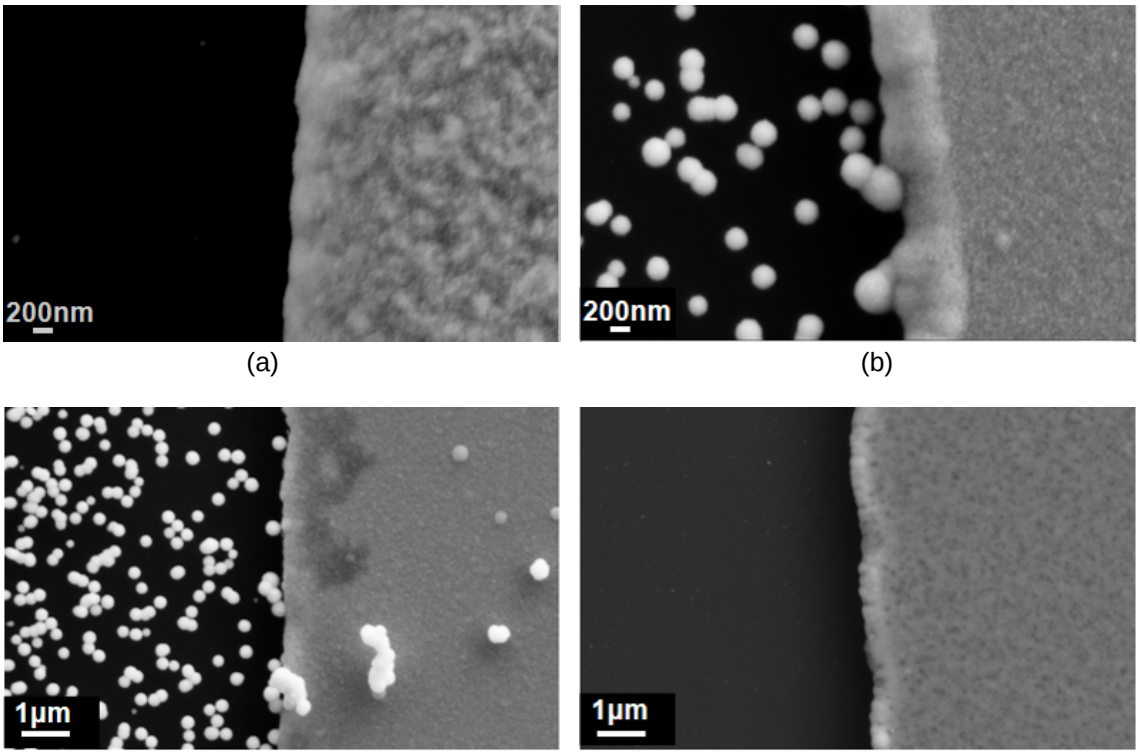

(a) (b)

(c) (d)

Figure 4.12 SEM micrographs of Au nanoparticles formation from self-prepared gold(I) sulfite electrolytes with the addition of Ni^{2+} ions at potential: (a) -0.4V; (b) -0.5V; (c) -0.6V; (d) -0.8V.

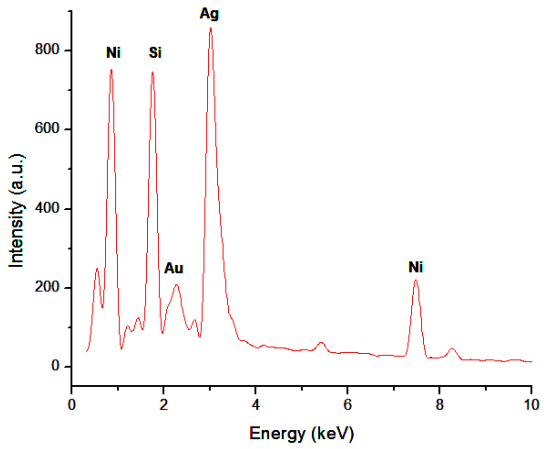

Figure 4.13 EDS data of electrochemically deposited thin film from self-prepared gold(I) electrolytes with Ni^{2+} ions at potential -0.8V.

4.3.3 Effects of Potential

Figure 4.14 shows that Au nanoparticles formed on the non-conductive areas from the gold(I) sulfite electrolytes with both EDA and Ni ions with different applied potentials. The average size of Au nanoparticles obtained at potential -0.6V is around 137nm in diameter. As the potential increased from -0.6V to -0.8V, in this case, the size of Au nanoparticles was increased from 137 nm to 171nm in diameter. It is known that hydrogen evolution is directly related to an applied potential, and Au^{+} is reduced at the hydrogen bubble boundary where electroless deposition occurs immediately after the formation of a stable bubble. It is expected that the higher potential the larger the Au nanoparticles.

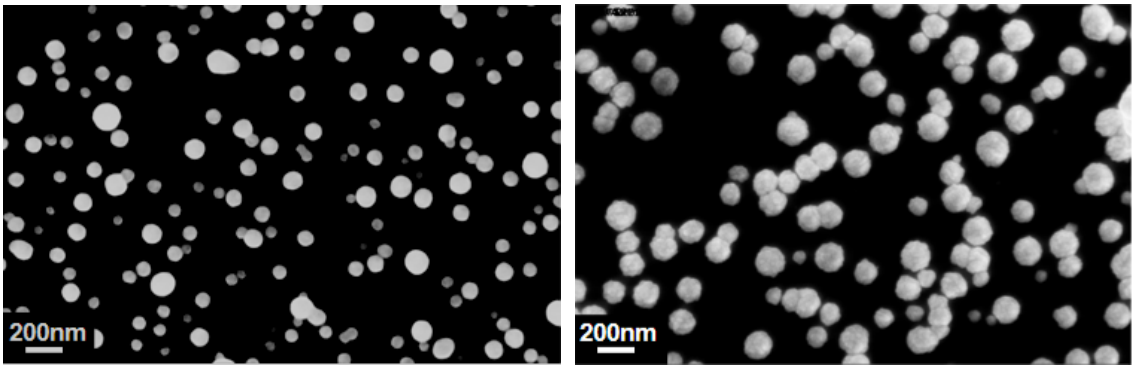

(a) (b)

Figure 4.14 SEM micrographs of Au nanoparticles formation on patterned substrates at: (a) potential -0.6V; (b) potential -0.8V.

Figure 4.15 shows that when potential -0.4V was applied, no Au nanoparticles on the non-conductive areas and very rough deposits on the metal strips, which may be caused by electroless deposition since the applied potential was more positive than the reduction potential of Au^{+}. The Au particles with irregular shape obtained at potential -0.5V may be due to an initial stage of hydrogen evolution.

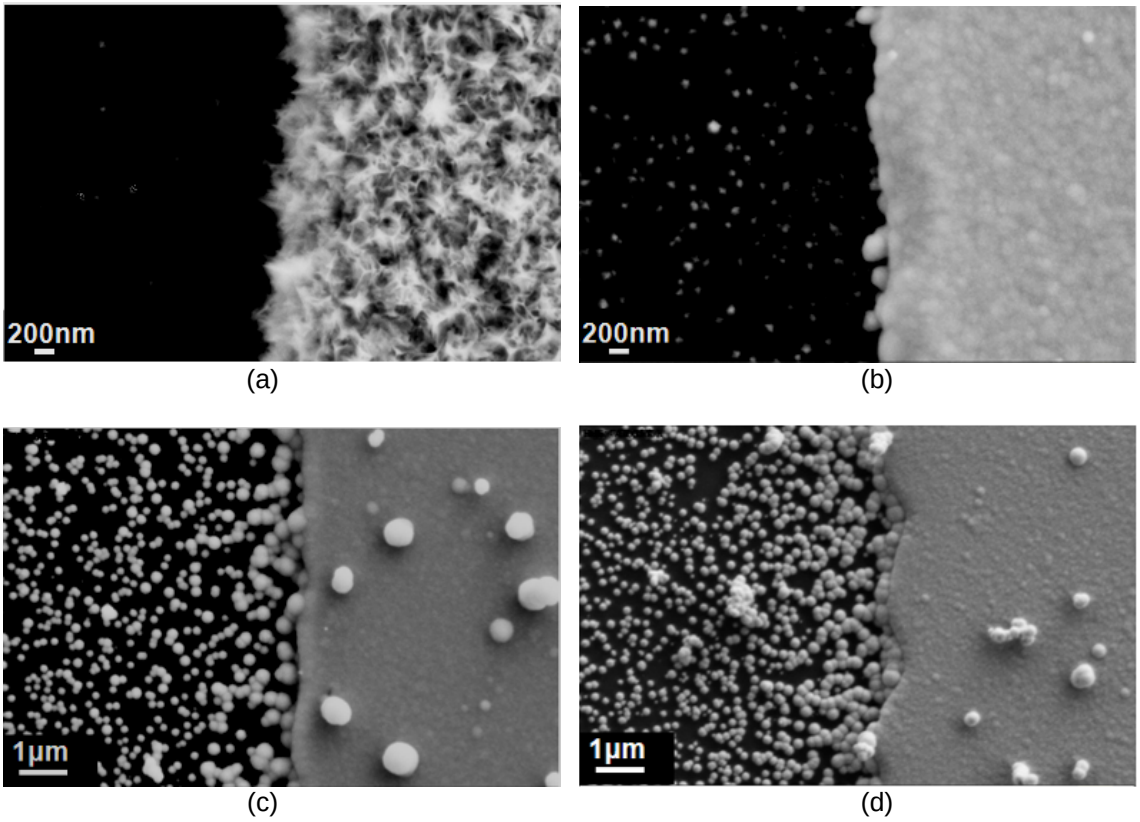

Figure 4.15 SEM micrographs of Au nanoparticles formation from self-prepared gold(I) sulfite electrolytes with the addition of EDA and Ni^{2+} ions at potential: (a) -0.4V; (b) -0.5V; (c) -0.6V; (d) -0.8V.

4.3.4 Effects of Hydrophobicity of Substrate

According to the existing theory, hydrophobicity of surfaces should have effects on the formation of gas bubbles, and these bubbles should not form on the hydrophilic surfaces. In this section, we investigated the formation of Au nanoparticles on different surfaces with various hydrophobicities.

The following substrates were used: porous anodic alumina oxide, flat alumina oxide, glass and Si wafer. Periodically patterned Ag strips were deposited on these substrates. Figure 4.16 shows the contact angle of water drops on the substrates. We can see among these substrates, porous anodic alumina oxide and flat alumina oxide substrates are highly hydrophilic, glass substrate is hydrophilic, and Si wafer is nearly hydrophobic.

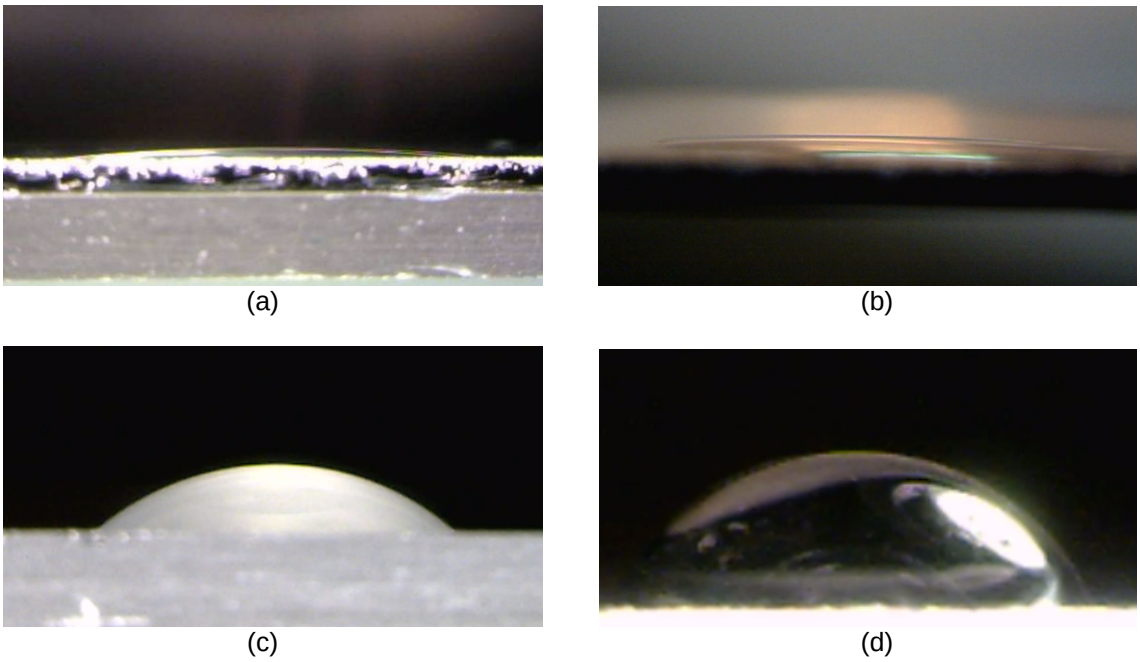

Figure 4.16 Images of small water drops on: (a) porous alumina oxide substrate; (b) flat alumina oxide substrate; (c) glass substrate; (d) Si wafer substrate.

On the highly hydrophilic porous anodic alumina oxide substrate, Au nanoparticles with a wide range of size formed, as shown in Figure 4.17a. In this case, the formation of hydrogen nanobubbles may be attributed to its rough surface which helps hydrogen molecules reach critical nucleus size. To verify this assumption, the highly hydrophilic flat alumina oxide substrate was utilized. Figure 4.17b shows that Au particles did also form on the flat alumina oxide surface. The results suggest that a high concentration of hydrogen molecules was able to form nanobubbles at the interface between hydrophilic solid and liquid. In addition, hydrophilic glass substrate was investigated as well. Figure 4.17c again shows Au nanoparticles could be generated on this hydrophilic surface. These results contradict our current understanding on bubble generation mechanism. Nanobubble generation on hydrophilic surfaces has been reported [61] , but the mechanism is still unknown. Figure 4.17d shows Au nanoparticles formed on the hydrophobic Si wafer surface, suggesting that the hydrogen nanobubble could exist on

hydrophobic solid/liquid interface which is expected. These results indicate that nanobubbles could be formed on both hydrophobic and hydrophilic surfaces.

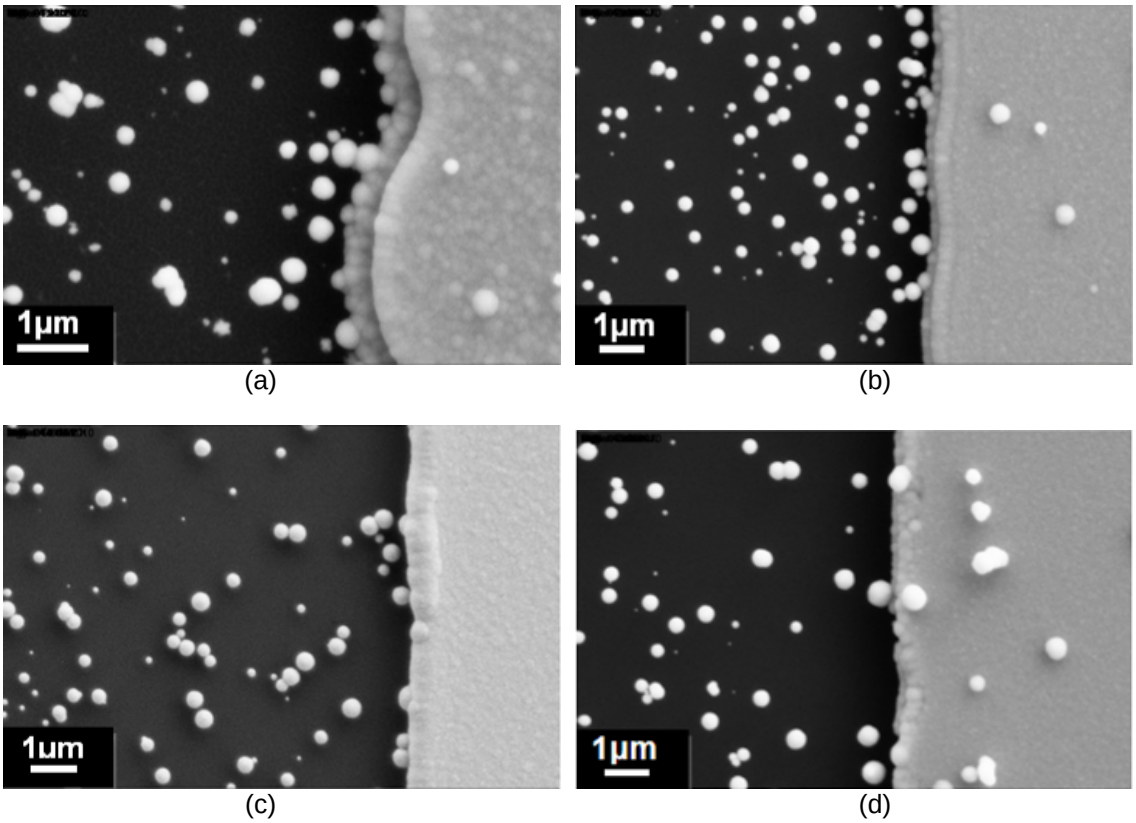

(a) (b)

(c) (d)

Figure 4.17 SEM micrographs of Au nanoparticles formation from self-prepared gold(I) sulfite solution with EDA at potential -0.6V on: (a) porous anodic alumina oxide substrate; (b) flat alumina oxide substrate; (c) glass substrate; (d) Si wafer substrate.

Not only, the hydrophobicity has little effect on generation of Au nanoparticles on different substrates, but also the contact angle of Au nanoparticles on different substrates with various hydrophobicities is not affected, as shown in Figure 4.18. This suggests that the formation of nanobubbles is very different from microscale gas bubbles, and more studies are needed.

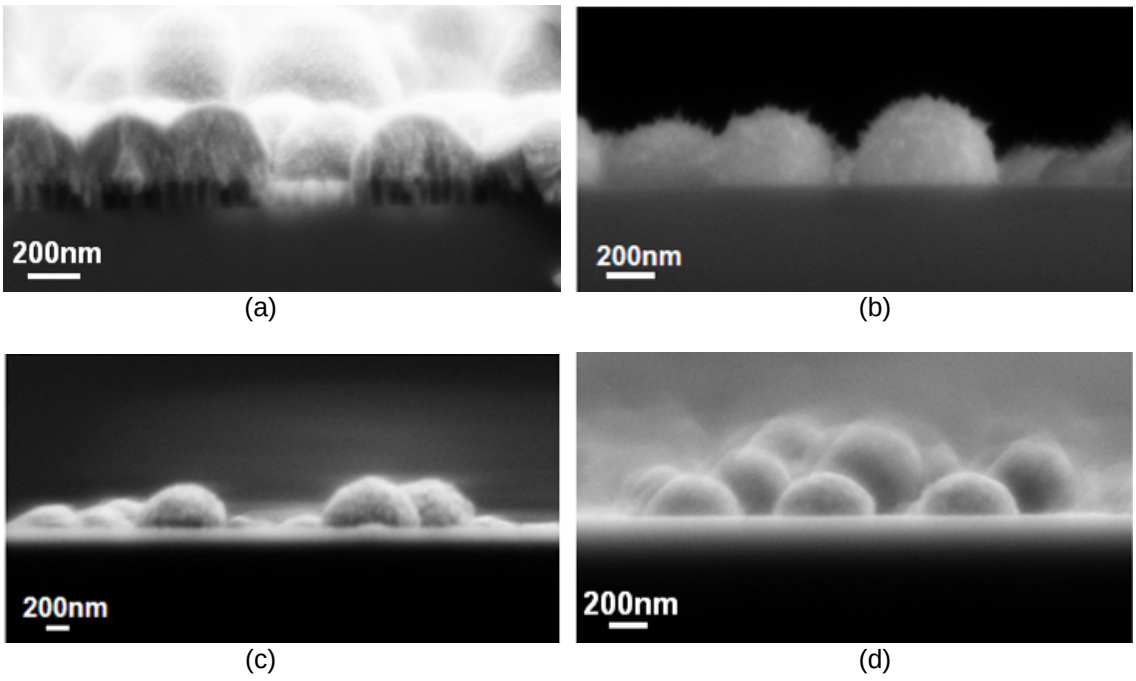

(a) (b)

(c) (d)

Figure 4.18 SEM micrographs of Au particles in front view on: (a) porous alumina oxide substrate; (b) flat alumina oxide substrate; (c) glass substrate; (d) Si wafer substrate.

4.4 Observation of Au Nanoparticle Formation on TEM Grid

Au nanoparticles were directly generated on TEM grid which provided a convenient way for analyzing the structure of Au nanoparticles. The hollow nature of Au nanoparticles was revealed by high-resolution transmission electron microscopy (HRTEM).

TEM grid illustrates in Figure 4.19a, consists of copper meshes with a heavy layer of carbon film. They were directly used as working electrode. Figure 4.19b shows that a large number of Au nanoparticles were formed on carbon film. This suggests that electrochemically evolved hydrogen bubbles were trapped on the carbon film, which reduces the Au ions into Au nanoparticles.

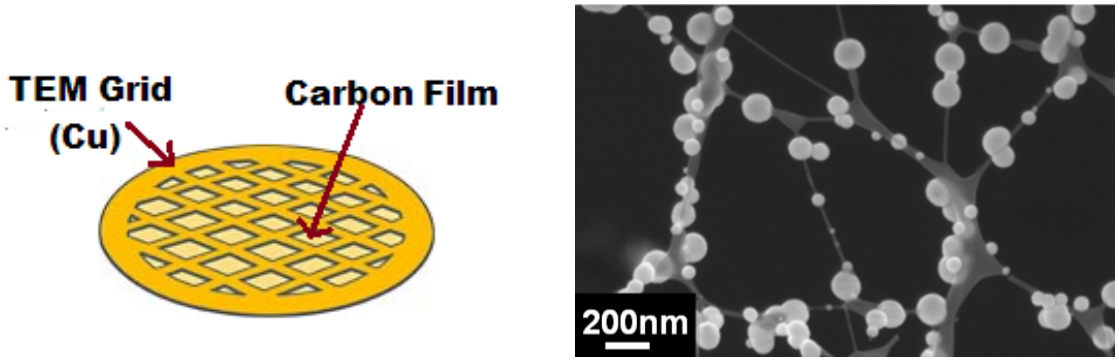

(a) (b)

Figure 4.19 (a) Illustration of TEM grid consists of copper meshes and carbon film; (b) SEM micrographs of Au nanoparticles on carbon film.

The TEM images were taken after the electrodeposition without any treatment. Figure 4.20a clearly indicates the hollow feature of Au nanoparticles, showing the hollow core with the radius of 25nm. This hollow feature again suggests that hydrogen bubbles acted as templates for the formation of Au nanoparticles.

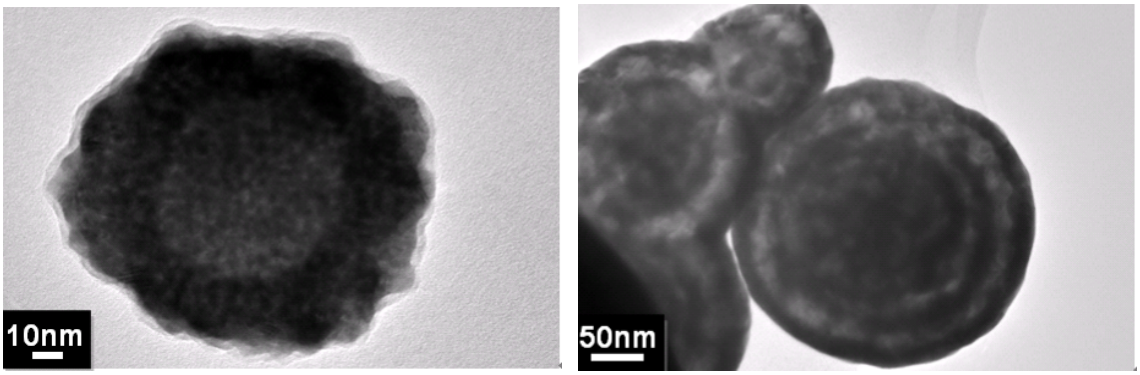

(a) (b)

Figure 4.20 TEM micrographs of: (a) hollow feature of Au nanoparticles; (b) a multiple-shell Au nanoparticles.

Unexpectedly, we also found that some of the Au nanoparticles with a multilayer structure, as shown in Figure 4.20b. The possible route for the formation of these multiple-shell Au nanoparticles can be considered as following. After an Au nanoparticle formed, another hydrogen bubbles formed and covered the existed Au nanoparticle. Au ions were thereafter

reduced by large hydrogen bubble to form other shell. This shell formation may able to be repeated many cycles.

4.5 Reduction of Au^{+} by Electrochemically Evolved Hydrogen Gas Bubbles

Au metal formed around electrochemically evolved hydrogen bubbles has also been directly observed. The assumption that electrochemically evolved hydrogen bubbles can serve as both templates and reducing agents has been confirmed.

Figure 4.21a illustrates this process. The hydrogen bubbles were electrochemically generated in the gold(I) sulfite electrolytes, and these bubbles were surrounded by a large amount of hydrogen molecules. These hydrogen molecules attempt to attach to the surface of the bubbles in the solution, reducing the Au ions into metallic Au by transferring electrons. This reduction reaction was directly observed in an experiment where we used an Au-coated silicon wafer as the working electrode. When a high negative potential (from -0.9 to -1.1V) was applied, hydrogen bubbles were generated at the working electrode surface and could be seen rising upward to the electrolyte surface. Pieces of metal debris which floated on the electrolyte surface were collected for analysis. Scanning electron micrographs (Figure 4.22) and energy dispersive X-ray spectroscopy confirmed that the debris is comprised of bowl-shaped Au nanoparticles, indicating that metallic Au indeed form at the bubble boundary. There are two possible Au formation mechanisms. First, a high concentration of molecular hydrogen may be able to reduce the Au+ into metal Au to form Au clusters, then the Au clusters act as catalyst to trigger the disproportionation reaction and more metal Au forms. Another possibility is that the hydrogen bubbles act as catalytic supports, just like metallic Au, for the disproportionation reaction to take place.

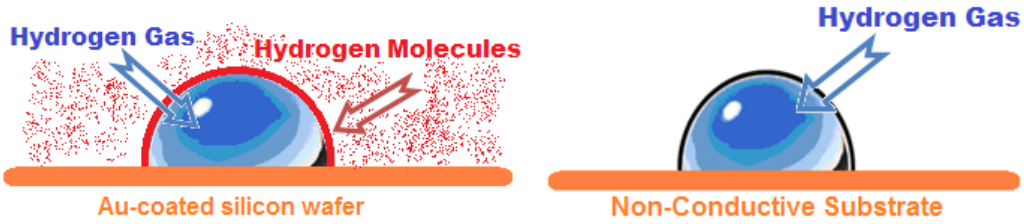

Figure 4.21 Illustration of: (a) the electrochemically evolved hydrogen bubbles in the hydrogen molecules rich gold(I) sulfite electrolytes; (b) hydrogen gas bubbles in the gold(I) sulfite electrolytes without external electric current.

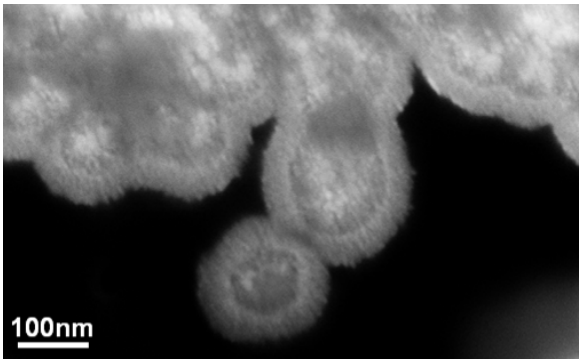

Figure 4.22 SEM micrograph showing the bowl-shape Au nanoparticles collected from the electrolytes surface.

We also tried to generate hydrogen gas bubble by directly bubbling pure hydrogen gas into the electrolyte solution. However, even at the same condition as for electrochemically generated bubbles, no reaction was observed on the boundary of these hydrogen gas bubbles. The possible reason could be that the hydrogen gas bubbles are less reactive than fresh electrochemically evolved hydrogen bubbles.

CHAPTER 5

CONCLUSION

In a series of experiments, Au nanoparticles have been successfully generated on the non-conductive areas from $Na_3Au(SO_3)_2$ electrolytes when a potential more negative than hydrogen evolution potential is applied, suggesting electroless deposition and hydrogen evolution play important roles in the Au nanoparticle formation. Au nanoparticles have also been produced on TEM grid which provides a convenient way for structural analysis. The hollow nature of Au nanoparticles was revealed by HRTEM, supporting the assumption that hydrogen bubbles can act as both templates and reducing agents. The assumption was also confirmed by direct evidence that the reduction of Au^+ happen around electrochemically evolved hydrogen bubbles.

The formation of Au nanoparticles can be described in three stages: (I) electrochemically evolved hydrogen bubbles; (II) reduction of Au^+ around hydrogen gas bubbles; (III) autocatalytic disproportionation reaction. The effects of different parameters on Au nanoparticles have been investigated. (1) The addition of either EDA or Ni^{2+} ion or both is the necessary condition for Au nanoparticle formation. EDA has capability to enhance the stability of gold(I) sulfite electrolytes and clean surface oxides of electrode to enhance hydrogen evolution efficiency; electrodeposited metal Ni can also enhance hydrogen evolution efficiency. It has also been found that the addition of Ni^{2+} ions can improve the size distribution of Au nanoparticles. (2) The electrodeposition potential directly affects the size of Au nanoparticles which is believed to be associated with hydrogen evolution; (3) Hydrophobicity of solid surface does not have effect on the formation and contact angle of Au nanoparticles which is not fully understood, and requires more studies on the mechanism of nanobubble formation.

APPENDIX A

THE NERNST EQUATION [87]

The Nernst equation is used to calculate the potential of an electrochemical cell as a function of ions taking part in the reaction. It can also be used to determine the total potential for a full electrochemical cell, but real voltaic cells will typically differ from the standard conditions. The two equations for these two cases, half-cell and full cell are as follows:

$$E_{red} = E_{red'} - \frac{RT}{zF} \ln \frac{a_{Red}}{a_{Ox}}$$ (half-cell reduction potential) (1)

$$E_{cell} = E_{cell'} - \frac{RT}{zF} \ln Q$$ (total cell potential) (2)

where $E_{red'}$ is the standard half-cell reduction potential; $E_{cel'l}$ is the standard cell potential; R is the universal gas constant (8.314 $JK^{-1}mol^{-1}$); T is the absolute temperature (K); a is the chemical activity for the relevant species; F is the Faraday constant (F = $9.648*10^4$ C mol^{-1}); z is the number of electrons transferred in the reaction; Q is the reaction quotient.

Energy drives all changes including chemical reactions. In a redox reaction, the energy released in a reaction due to movement of charged particles gives rise to a potential difference. The maximum potential difference is the electromotive force (E); the maximum electric work (W) is the product of charge q in Coulomb (C), and the potential △E in Volt (J/C).

WJ = q△ECJ/C (units) (3)

Note that the △E is determined by the nature of the reactants and electrolytes, not by the size of the cell.

The Gibb's free energy (△G) is the negative value of maximum electric work.

△G = -W = -q△E (4)

A redox reaction equation represents definite amounts of reactants in the formation. The number (n) of electrons in a reaction equation is related to the amount of charge transferred.

q = n F (5)

At standard conditions,

△G°= -nF △E° (6)

The general Nernst equation correlates the Gibb's Free Energy and the △E of a chemical system known as the galvanic cell. For the reaction

$$Q = \frac{[C]^c\,[D]^d}{[A]^a\,[B]^b} \tag{8}$$

This is the more general form of the Nernst equation. For the redox reaction

$$Ox + nc^- \rightarrow Red,\ Q = \frac{[Red]}{[Ox]} \tag{9}$$

It has been shown that

$$\triangle G = \triangle G^\circ + RT\ln Q \tag{10}$$

and

$$\triangle G = -\,n\,F\triangle E \tag{11}$$

Therefore

$$-\,nF\triangle E = -\,nF\triangle E^\circ + RT\ln Q \tag{12}$$

This is known as the Nernst equation. The equation allows us to calculate the cell potential of any galvanic cell for any concentrations.

According to the Nernst equation, hydrogen evolution was calculated and occurs electrochemically at room temperature (25℃). At ro om temperature, RT/F may be treated like a constant and replaced by 25.693 mV for cells. The Nernst equation is frequently expressed in terms of base 10 rather than natural logarithms, in which case it is written, for a cell at 25 ℃:

$$E = E^{\upsilon} - \frac{0.05916\ V}{z}\log_{10}\frac{a_{Red}}{a_{Ox}} \tag{13}$$

REFERENCES

1. Ohmori, T., *Role of a surface disruption of electrode in electrochemical characteristics.1.influence of a surface disruption of electrode on the rate of the hydrogen evolution reaction.* Journal of Electroanalytical Chemistry, 1984. **172**(1-2): p. 123-130.
2. Link, S. and M.A. El-Sayed, *Spectral properties and relaxation dynamics of surface plasmon electronic oscillations in gold and silver nanodots and nanorods.* Journal of Physical Chemistry B, 1999. **103**(40): p. 8410-8426.
3. Creighton, J.A. and D.G. Eadon, *Ultraviolet visible absorption-spectra of the colloidal metallic elements.* Journal of the Chemical Society-Faraday Transactions, 1991. **87**(24): p. 3881-3891.
4. Wang, Z.L., *Transmission electron microscopy of shape-controlled nanocrystals and their assemblies.* Journal of Physical Chemistry B, 2000. **104**(6): p. 1153-1175.
5. Hu, J.T., T.W. Odom, and C.M. Lieber, *Chemistry and physics in one dimension: Synthesis and properties of nanowires and nanotubes.* Accounts of Chemical Research, 1999. **32**(5): p. 435-445.
6. Jain, P.K., et al., *Review of some interesting surface plasmon resonance-enhanced properties of noble metal nanoparticles and their applications to biosystems.* Plasmonics, 2007. **2**(3): p. 107-118.
7. Li, M., et al., *Optical properties of Au/Ag core/shell nanoshuttles.* Optics Express, 2008. **16**(18): p. 14288-14293.
8. Daniel, M.C. and D. Astruc, *Gold nanoparticles: Assembly, supramolecular chemistry, quantum-size-related properties, and applications toward biology, catalysis, and nanotechnology.* Chemical Reviews, 2004. **104**(1): p. 293-346.
9. Yu, Y.Y., et al., *Gold nanorods: Electrochemical synthesis and optical properties.* Journal of Physical Chemistry B, 1997. **101**(34): p. 6661-6664.
10. Foss, C.A., et al., *Template-synthesized nanoscopic gold particles - optical-spectra and the effects of particle-size and shape.* Journal of Physical Chemistry, 1994. **98**(11): p. 2963-2971.
11. Skrabalak, S.E., et al., *Facile synthesis of Ag nanocubes and Au nanocages.* Nature Protocols, 2007. **2**(9): p. 2182-2190.
12. Liang, Z.J., A. Susha, and F. Caruso, *Gold nanoparticle-based core-shell and hollow spheres and ordered assemblies thereof.* Chemistry of Materials, 2003. **15**(16): p. 3176-3183.
13. Shevchenko, E.V., et al., *Gold/Iron Oxide Core/Hollow-Shell Nanoparticles.* Advanced Materials, 2008. **20**(22): p. 4323-4329.
14. Vasquez, Y., et al., *Nanocrystal conversion chemistry: A unified and materials-general strategy for the template-based synthesis of nanocrystalline solids.* Journal of Solid State Chemistry, 2008. **181**(7): p. 1509-1523.
15. Turkevitch, J., P.C. Stevenson, and J. Hillier, *Nucleation and growth process in the synthesis of colloidal.* Discuss.Faraday Soc., 1951. **11**.
16. Frens, G., *Controlled nucleation for regulation of particle-size in monodisperse gold suspensions.* Nature-Physical Science, 1973. **241**(105): p. 20-22.
17. Brust, M., et al., *Synthesis of thiol-derivatized gold nanoparticles in a 2-phase liquid-liquid system.* Journal of the Chemical Society-Chemical Communications, 1994(7): p. 801-802.

18. Sun, L., R.M. Crooks, and V. Chechik, *Preparation of polycyclodextrin hollow spheres by templating gold nanoparticles.* Chemical Communications, 2001(4): p. 359-360.
19. Cepak, V.M. and C.R. Martin, *Preparation and stability of template-synthesized metal nanorod sols in organic solvents.* Journal of Physical Chemistry B, 1998. **102**(49): p. 9985-9990.
20. Esumi, K., K. Matsuhisa, and K. Torigoe, *Preparation of rodlike gold particles by uv irradiation using cationic micelles as a template.* Langmuir, 1995. **11**(9): p. 3285-3287.
21. Van der Zande, B.M.I., et al., *Colloidal dispersions of gold rods: Synthesis and optical properties.* Langmuir, 2000. **16**(2): p. 451-458.
22. Fullam, S., et al., *Carbon nanotube templated self-assembly and thermal processing of gold nanowires.* Advanced Materials, 2000. **12**(19): p. 1430-1432.
23. Jana, N.R., L. Gearheart, and C.J. Murphy, *Evidence for seed-mediated nucleation in the chemical reduction of gold salts to gold nanoparticles.* Chemistry of Materials, 2001. **13**(7): p. 2313-2322.
24. Jana, N.R., L. Gearheart, and C.J. Murphy, *Seeding growth for size control of 5-40 nm diameter gold nanoparticles.* Langmuir, 2001. **17**(22): p. 6782-6786.
25. Henglein, A. and M. Giersig, *Formation of colloidal silver nanoparticles: Capping action of citrate.* Journal of Physical Chemistry B, 1999. **103**(44): p. 9533-9539.
26. Perez-Juste, J., et al., *Gold nanorods: Synthesis, characterization and applications.* Coordination Chemistry Reviews, 2005. **249**(17-18): p. 1870-1901.
27. F. Fievet, J.P.L., M. Figlarz, *Preparing monodisperse metal powers in micrometer and submicrometer sizes by the polyol process.* MRS Bulletin, 1989(14): p. 29.
28. Chen, J., et al., *Gold nanocages: Bioconjugation and their potential use as optical imaging contrast agents.* Nano Letters, 2005. **5**(3): p. 473-477.
29. Au, L., et al., *Quantifying the cellular uptake of antibody-conjugated Au nanocages by two-photon microscopy and inductively coupled plasma mass spectrometry.* Acs Nano. **4**(1): p. 35-42.
30. Rycenga, M., et al., *Probing the surface-enhanced Raman scattering properties of Au-Ag nanocages at two different excitation wavelengths.* Physical Chemistry Chemical Physics, 2009. **11**(28): p. 5903-5908.
31. Gates, B. and Y.N. Xia, *Fabrication and characterization of chirped 3D photonic crystals.* Advanced Materials, 2000. **12**(18): p. 1329-1332.
32. Shi, W.L., et al., *Gold nanoshells on polystyrene cores for control of surface plasmon resonance.* Langmuir, 2005. **21**(4): p. 1610-1617.
33. Halas, N., *Playing with plasmons. Tuning the optical resonant properties of metallic nanoshells.* Mrs Bulletin, 2005. **30**(5): p. 362-367.
34. Neeves, A.E. and M.H. Birnboim, *Composite structures for the enhancement of nonlinear-optical susceptibility.* Journal of the Optical Society of America B-Optical Physics, 1989. **6**(4): p. 787-796.
35. Averitt, R.D., S.L. Westcott, and N.J. Halas, *Linear optical properties of gold nanoshells.* Journal of the Optical Society of America B-Optical Physics, 1999. **16**(10): p. 1824-1832.
36. Kerker, M., D.S. Wang, and H. Chew, *Surface enhanced Raman-scattering (SERS) by molecules adsorbed at spherical-oarticles.* Applied Optics, 1980. **19**(24): p. 4159-4174.
37. Olofsson, L., et al., *Surface-based gold-nanoparticle sensor for specific and quantitative DNA hybridization detection.* Langmuir, 2003. **19**(24): p. 10414-10419.
38. Cho, E.C., et al., *Measuring the Optical Absorption Cross Sections of Au-Ag Nanocages and Au Nanorods by Photoacoustic Imaging.* Journal of Physical Chemistry C, 2009. **113**(21): p. 9023-9028.
39. Gobin, A.M., et al., *Near-infrared resonant nanoshells for combined optical imaging and photothermal cancer therapy.* Nano Letters, 2007. **7**(7): p. 1929-1934.

40. Qian, X.M., et al., *In vivo tumor targeting and spectroscopic detection with surface-enhanced Raman nanoparticle tags.* Nature Biotechnology, 2008. **26**(1): p. 83-90.
41. Sharrna, P., et al., *Nanoparticles for bioimaging.* Advances in Colloid and Interface Science, 2006. **123**: p. 471-485.
42. Niidome, T., et al., *In vivo monitoring of intravenously injected gold nanorods using near-infrared light.* Small, 2008. **4**(7): p. 1001-1007.
43. Kato, M., et al., *Substrate (Ni)-catalyzed electroless gold deposition from a noncyanide bath containing thiosulfate and sulfite - I. Reaction mechanism.* Journal of the Electrochemical Society, 2002. **149**(3): p. C164-C167.
44. Liew, M.J., S. Roy, and K. Scott, *Development of a non-toxic electrolyte for soft gold electrodeposition: an overview of work at University of Newcastle upon Tyne.* Green Chemistry, 2003. **5**(4): p. 376-381.
45. Kato, M. and Y. Okinaka, *Some recent developments in non-cyanide gold plating for electronics applications.* Gold Bulletin, 2004. **37**(1-2): p. 37-44.
46. Green, T.A. and S. Roy, *Speciation analysis of Au(I) electroplating baths containing sulfite and thiosulfate.* Journal of the Electrochemical Society, 2006. **153**(3): p. C157-C163.
47. Mordechay Schlesinger, M.P., *Modern electroplating*. 4th ed. 2000: Wiley interscience.
48. Honma, H. and Y. Kagaya, *Gold plating using the disulfiteaurate complex.* Journal of the Electrochemical Society, 1993. **140**(9): p. L135-L137.
49. Okinaka, Y. and M. Hoshino, *Some recent topics in gold plating for electronics applications.* Gold Bulletin, 1998. **31**(1): p. 3-13.
50. Honma, H., et al., *Electroless gold plating by disulfiteaurate complex.* Plating and Surface Finishing, 1995. **82**(4): p. 89-92.
51. Morrissey, R.J., *Non-cyanide electroplating solution for gold or alloys thereof*, US, Editor. 1994: USA.
52. P. Laude, E.M., and Z. Morrens, *Aqueous solution of monovalent gold and ammonium sulfite complex, process for the preparation thereof and electrolytic bath obtained therefrom for the plating of gold or gold alloy**s*** in *U.S. Patent 4,192,723* U. Patent, Editor. 1980: USA.
53. He, A., Q. Liu, and D.G. Ivey, *Electroplating of gold from a solution containing tri-ammonium citrate and sodium sulphite.* Journal of Materials Science-Materials in Electronics, 2009. **20**(6): p. 543-550.
54. Green, T.A., M.J. Liew, and S. Roy, *Electrodeposition of gold from a thiosulfate-sulfite bath for microelectronic applications.* Journal of the Electrochemical Society, 2003. **150**(3): p. C104-C110.
55. Osaka, T., et al., *Electrodeposition of soft gold from a thiosulfate-sulfite bath for electronics applications.* Journal of the Electrochemical Society, 1997. **144**(10): p. 3462-3469.
56. Liew, M.J., S. Sobri, and S. Roy, *Characterisation of a thiosulphate-sulphite gold electrodeposition process.* Electrochimica Acta, 2005. **51**(5): p. 877-881.
57. Ljunggren, S. and J.C. Eriksson, *The lifetime of a colloid-sized gas bubble in water and the cause of the hydrophobic attraction.* Colloids and Surfaces a-Physicochemical and Engineering Aspects, 1997. **130**: p. 151-155.
58. Brenner, M.P. and D. Lohse, *Dynamic equilibrium mechanism for surface nanobubble stabilization.* Physical Review Letters, 2008. **101**(21): p. 4.
59. Tyrrell, J.W.G. and P. Attard, *Images of nanobubbles on hydrophobic surfaces and their interactions.* Physical Review Letters, 2001. **87**(17): p. 4.
60. Zhang, X.H., N. Maeda, and V.S.J. Craig, *Physical properties of nanobubbles on hydrophobic surfaces in water and aqueous solutions.* Langmuir, 2006. **22**(11): p. 5025-5035.

61. Zhang, X.H., et al., *Degassing and temperature effects on the formation of nanobubbles at the mica/water interface.* Langmuir, 2004. **20**(9): p. 3813-3815.
62. Yang, S.J., et al., *Characterization of nanobubbles on hydrophobic surfaces in water.* Langmuir, 2007. **23**(13): p. 7072-7077.
63. Zhang, X.H., A. Quinn, and W.A. Ducker, *Nanobubbles at the interface between water and a hydrophobic solid.* Langmuir, 2008. **24**(9): p. 4756-4764.
64. Attard, P., *Nanobubbles and the hydrophobic attraction.* Advances in Colloid and Interface Science, 2003. **104**: p. 75-91.
65. Tyrrell, J.W.G. and P. Attard, *Atomic force microscope images of nanobubbles on a hydrophobic surface and corresponding force-separation data.* Langmuir, 2002. **18**(1): p. 160-167.
66. Lou, S.T., et al., *Nanobubbles on solid surface imaged by atomic force microscopy.* Journal of Vacuum Science & Technology B, 2000. **18**(5): p. 2573-2575.
67. Attard, P., M.P. Moody, and J.W.G. Tyrrell, *Nanobubbles: the big picture.* Physica a-Statistical Mechanics and Its Applications, 2002. **314**(1-4): p. 696-705.
68. Agrawal, A., et al., *Controlling the location and spatial extent of nanobubbles using hydrophobically nanopatterned surfaces.* Nano Letters, 2005. **5**(9): p. 1751-1756.
69. Switkes, M. and J.W. Ruberti, *Rapid cryofixation/freeze fracture for the study of nanobubbles at solid-liquid interfaces.* Applied Physics Letters, 2004. **84**(23): p. 4759-4761.
70. Steitz, R., et al., *Nanobubbles and their precursor layer at the interface of water against a hydrophobic substrate.* Langmuir, 2003. **19**(6): p. 2409-2418.
71. Zhang, X.H., A. Khan, and W.A. Ducker, *A nanoscale gas state.* Physical Review Letters, 2007. **98**(13).
72. Ishida, N., et al., *Nano bubbles on a hydrophobic surface in water observed by tapping-mode atomic force microscopy.* Langmuir, 2000. **16**(16): p. 6377-6380.
73. Nam, Y. and Y.S. Jua, *Bubble nucleation on hydrophobic islands provides evidence to anomalously high contact angles of nanobubbles.* Applied Physics Letters, 2008. **93**(10).
74. Zhang, L.J., et al., *Electrochemically controlled formation and growth of hydrogen nanobubbles.* Langmuir, 2006. **22**(19): p. 8109-8113.
75. Fernando, C.A.N. and S.K. Wetthasinghe, *Investigation of photoelectrochemical characteristics of n-type Cu2O films.* Solar Energy Materials and Solar Cells, 2000. **63**(3): p. 299-308.
76. Lacovangelo, C.D. and K.P. Zarnoch, *Substrate-catalyzed electroless gold plating* Journal of the Electrochemical Society, 1991. **138**(4): p. 983-988.
77. Porter, L.A., et al., *Controlled electroless deposition of noble metal nanoparticle films on germanium surfaces.* Nano Letters, 2002. **2**(10): p. 1067-1071.
78. Sato, J., et al., *Substrate (Ni)-catalyzed electroless gold deposition from a noncyanide bath containing thiosulfate and sulfite - II. Deposit characteristics and substrate effects.* Journal of the Electrochemical Society, 2002. **149**(3): p. C168-C172.
79. Oskam, G., et al., *Electrochemical deposition of metals onto silicon.* Journal of Physics D-Applied Physics, 1998. **31**(16): p. 1927-1949.
80. Hawkins, A.R. *Contact photolithographic alignment tutorial*. 2004; Available from: http://cleanroom.byu.edu/alignment.phtml.
81. Jaksic, M.M., B. Johansen, and R. Tunold, *Electrochemical behavior of palladium in acidic and alkaline solutions of heavy regular water* International Journal of Hydrogen Energy, 1993. **18**(2): p. 111-124.
82. Kibria, A.K.M.F., *Effect of ethylene diamine tetra acetic acid (EDTA) on the surface reaction behavior and the hydrogen evolution efficiency of Ni-30at. %Cu electrode in alkaline medium.* Bangladesh Journal of Scientific and Industrial Research, 2008. **43**(2): p. 145-158.

83. Vandeberg, P.J. and D.C. Johnson, *A study of the voltammetric response of thiourea and ethylene thiourea at gold electrode in alkaline media.* Journal of Electroanalytical Chemistry, 1993. **362**(1-2): p. 129-139.
84. Jaksic, M.M., et al., *The Rowland or EDTA effect on electrochemical behavior of transition metals and in electrocatalysis for the hydrogen evolution reaction. The Rowland effect on some non-noble non-valve transition metals.* Russian Journal of Electrochemistry, 1995. **31**(11): p. 1187-1202.
85. Sawyer, D.T., A. Sobkowiak, and J.L. Roberts, *Electrochemistry for chemists*, ed. 2nd. 1995.
86. Boateng, D.A., et al., *Production of nickel by hydrogen reduction of nickel-loaded organic acid solution.* Ind. Eng. Chem. Process Des. Dev., 1981. **20**.
87. Orna, M.V. and J. Stock, *Electrochemistry, past and present*. 1989, Columbus, OH: American Chemical Society.

BIOGRAPHICAL INFORMATION

Yijiun Li was born in Taipei, Taiwan. In 2004, he completed his bachelor degree from the Department of Polymer Engineering at National Taiwan University of Science and Technology in Taipei, Taiwan.

In the same year, he joined military police as obligation for one year and a half. After that, he worked in Foxconn as filed application engineer responsible for desktop and LED thermal solution. In order to purchase more knowledge in materials, he joined the Department of Materials Science and Engineering at the University of Texas at Arlington in 2008 pursuing a master degree. He worked at the Metallic Nanostructure Laboratory for two years as research assistant. His research area covers Anodic Alumina oxide, nanoscale hydrogen evolution, and hollow Au nanoparticles. After completion of master's degree, he will look for an engineer position in nanomaterials-related areas.